Control Engineering Practice 21 (2013) 1488–1506

Contents lists available at ScienceDirect

Control Engineering Practice

journal homepage: www.elsevier.com/locate/conengprac

Control system design and evaluation for robust autonomous rotorcraft guidance

Navid Dadkhah, Bérénice Mettler*

Interactive Guidance and Control Lab, Department of Aerospace Engineering and Mechanics, University of Minnesota, Minneapolis, MN 55455, USA

ARTICLE INFO

Article history:
Received 21 December 2011
Accepted 28 April 2013
Available online 13 August 2013

Keywords:
Control system design
Experimental evaluation
Rotorcraft UAV
Guidance application

ABSTRACT

This paper describes the design and performance analysis of a control system for rotorcraft with an emphasis on the requirements called for by autonomous guidance. To be able to track trajectories, such as those generated by a guidance system, a path following controller is used in combination with a velocity control augmentation. The path following system is motivated by nonlinear stability analysis. The velocity control augmentation follows a loop-shaping design for the inner-loop attitude control and a dynamic inversion velocity control design for the outer-loop. The identified model of the dynamics along with the uncertainties is used to determine the robustness and performance of the velocity control system. Finally, the paper presents a novel method to evaluate the overall performance of the control system in terms of the tracking error statistics. These results are then used to determine a tracking error model, which can be used to predict the tracking error for a given reference.

1. Introduction

UAVs have started supplanting manned aircraft in a broad range of tasks. At the same time they are also redefining operational concepts and even extending the range of aerial applications. For example, vehicles such as miniature rotorcraft with broad maneuvering range and small size can enter remote locations that are hard to reach using other air and ground vehicles. Yet while envisioning these applications is straightforward, it is all too easy to overlook the many engineering and technological hurdles they contain. Typical tasks such as search, inspection, surveillance and exploration, are beyond today's control and guidance technology for confined operation. The shortcomings lie both in the design and available hardware, particularly in the area of sensing and perception.

Putting aside the sensory and hardware hurdles, fundamental aspects of control and guidance still require improvements beyond existing approaches until autonomous systems can achieve operational flexibility similar to that under human control. The coupled and multivariable dynamics of rotorcraft, in addition to high bandwidth requirements, present well known control design challenges. Autonomous operation adds yet another level of complexity that cannot be solved without analysis of the control system within the larger autonomous system architecture. Within an autonomous guidance system, the control system has the role of executing trajectories that are typically generated by a planning algorithm. Control design is responsible both for providing desirable dynamic response characteristics and tracking capabilities. Most of the control design methods are based on linearized dynamics, yet full-envelope autonomous guidance induces significant nonlinear and unsteady conditions. First, a versatile guidance system will generate trajectories that put the vehicle under a broad range of velocities and acceleration profiles. Second, more advanced autonomous guidance systems operate in a closed loop, which means that the trajectory is constantly being updated. Therefore, the control system and tracking controller must be able to handle changing operating points.

Current design methods, as well as testing and evaluation procedures, do not respond directly to the needs of autonomous guidance. Traditional concepts of control performance that are often employed in multivariable control do not provide a complete picture of the performance under nonlinear and unsteady operational conditions. Ultimately, to ensure reliable and versatile performance it is necessary to test the control performance under broad and realistic flight conditions. More comprehensive test data is necessary to identify shortcomings that do not manifest in traditional tests. The test data can then also be used to determine more comprehensive models of the overall system's control performance. Such models can then be used within the guidance system where they allow for the accounting of the tradeoff between performance and safety during operation in a way that is similar to human operation.

The concept of control performance within autonomous guidance is not clearly defined. The most comprehensive assessments

* Corresponding author. Tel.: +1 6126240529.
E-mail addresses: navidd@aem.umne.du (N. Dadkhah), mettler@aem.umn.edu (B. Mettler).

0967-0661/$ - see front matter © 2013 Elsevier Ltd. All rights reserved.
http://dx.doi.org/10.1016/j.conengprac.2013.04.011

of control augmentations pertain to crewed vehicle handling quality requirements (see e.g. U.S. Army Aviation & Missile Command, 2000). For unmanned rotorcraft, in most of the published work, the experimental or simulation results are limited to classic testing procedures based on step or doublet response. These assessments do not provide sufficient data to predict the overall tracking performance when operating within a guidance system.

This paper addresses the design problem of practical control laws for robust autonomous rotorcraft guidance. It focuses on the following issues and challenges: (1) particular dynamics and modeling uncertainties found in miniature helicopter; (2) control requirements called for by path following; (3) procedures to experimentally characterize the performance; and (4) modeling the tracking error and path following performance. The paper includes experimental results obtained from a miniature, coaxial Blade-CX2 helicopter. Most material is illustrated based on this platform; however, the general approach, in particular the path tracking system and performance modeling are relevant to other rotorcraft types and sizes.

The dynamic model of Blade-CX2 helicopter used in this paper was modeled using frequency-domain system identification techniques (see Dadkhah & Mettler, accepted for publication for detailed account). Frequency-domain identification has become a standard approach for helicopters across a broad range of scale (Mettler, 2002; Tischler & Remple, 2006). The extracted frequency responses and model data are suited for control design. In particular they provide information about the fidelity of the model across frequencies (via model matching and extracted coherence function), as well as the level of confidence in the identified model parameters (via the Cramer–Rao bounds, which provide a lower bound on the variance of the identified parameter). This statistical information is used to guide the design and analysis of the control system.

Miniature helicopters have several characteristic sources of modeling uncertainties that need to be accounted for during the control design. These include variations in platform dynamics due to changes in mechanical configuration. Low-cost miniature helicopters are built from lower-cost parts with larger tolerances and tend to get damaged during manipulations and hard landing. The dynamic behavior may also vary from one helicopter to another due to the large possible combination of mechanical disturbances (stabilizer bar, swash-plate, servo-actuators, shafts, motors, linkages, c.g. location, etc.).

The control design approach used in this paper is based on a nested architecture combining an inner attitude loop and an outer velocity control loop. Classical loop-shaping was applied to the inner attitude loop. The Blade-CX2 helicopter has a lightly damped Fuselage-Rotor-Stabilizer/bar (FRS) and Phugoid mode, which makes loop-shaping a sensible design method for this system. In addition, the experimental frequency responses were utilized directly in the loop-shaping procedure in order to reduce the effect of discrepancy between the nominal model and the experimental frequency responses. The system identification results show that a reduced order model accurately relates the attitude and velocity dynamics. This is due to the fact that the velocity states are much slower in responding to commands and disturbances than the rotor flapping or angular rate states. Thanks to this time-scale separation, dynamic inversion was applied for the outer velocity control loop.

Advanced guidance laws (see e.g. Dadkhah & Mettler, 2011; Mettler, Dadkhah, & Kong, 2010) generate a reference path specified by a sequence of waypoints and speeds. The control laws and guidance system are integrated through a path following architecture based on nonlinear path following stability analysis of the rigid-body dynamics. The overall path performance is evaluated using a new flight-test procedure based on a novel set of performance criteria that were developed to capture the requirements of autonomous guidance.

The subsequent sections are organized as follows. Section 2 provides an overview of the approach in this paper. Section 3 provides descriptions of the system dynamics and the uncertainty model for Blade-CX2 miniature helicopter. Section 4 discusses the control system architecture and robustness analysis. In Section 5.1 the experimental setup is described. Section 5 describes the control performance measures and testing method developed to experimentally evaluate control systems as part of the guidance system. Finally, Section 6 provides some concluding remarks.

2. Background and overview

2.1. Control design

A variety of control techniques for miniature rotorcraft have been proposed and flight tested. In Civita, Papageorgiou, Messner, and Kanade (2006) an H_∞ loop-shaping technique was used to design a nested flight control system based on attitude, velocity and position loops for a small-scale helicopter. In Halaas, Bieniawski, Pigg, and Vian (2009), a linear quadratic (LQ) design was used as a rapid control technique to control and flight test different types of VSTL miniature rotorcraft. In Michini and How (2009), an L_1 adaptive control was implemented for indoor experiments. Authors in Takahashi, Schulein, and Walley (2008) used a classical loop-shaping method with model-following techniques to design a control law for a small-scale helicopter. The controller was setup as an inner attitude loop with an outer velocity and position loop. The helicopter in Reference Johnson and Kannan (2002) was controlled using a neural network based adaptive flight controller that consisted of an inner attitude loop and outer trajectory control loop. The outer-loop was used to correct the commanded attitude in order to follow position and velocity commands. In Kim and Shim (2003) a hierarchical flight control system based on multi-loop PID method to track the desired position was designed. A nonlinear model predictive controller (MPC) was then applied to minimize the tracking error due to non-linearities over the flight envelope, as well as input/state saturation. In Mettler, Tischler, Kanade, and Messner (2000) a classical attitude controller using the identified model of the vehicle dynamics was designed. The controller was further optimized for performance using CONDUIT (Tischler et al., 1999) (Control Designer's Unified Interface) based on frequency response envelope specification. In Gavrilets, Martinos, Mettler, and Feron (2002) a multi-variable controller for acrobatic maneuvers was designed using a combination of model-based and Linear Quadratic (LQ) design techniques. Authors in Schafroth, Bermes, Bouabdallah, and Siegwart (2010) designed attitude and heave/yaw controllers for a small-scale coaxial helicopter. In their work, the identified nonlinear model of the helicopter was linearized around a hover operating point and then the controller was designed using mixed-sensitivity H_∞ optimization technique. In Enns and Keviczky (2006) nested attitude, velocity and position dynamic inversion loops, with feedforward acceleration and velocity commands, was designed and simulated for a small-scale helicopter.

2.2. Path tracking design

In typical autonomous guidance applications the control systems are ultimately used for tracking a reference path. Two types of approaches can be distinguished for the tracking problem (Aguiar & Hespanha, 2007; Encarnaçao & Pascoal, 2001): *Trajectory Tracking*, where the vehicle is required to track a time-parametrized reference, and *Path Following* where the vehicle is

required to converge to follow a desired path without a temporal law while tracking a desired speed profile. Theoretical studies showed that in path following smoother convergence to the path and less demand on control effort is achieved (Aguiar, Dačić, Hespanha, & Kokotović, 2004; Aguiar, Hespanha, & Kokotović, 2005). Classical trajectory tracking approaches include designing position control loops that are able to follow a commanded position (see e.g. Civita et al., 2006; Enns & Keviczky, 2006; Kim, Shim, & Sastry, 2002; Takahashi et al., 2008). Alternative modern approaches utilize the linear or nonlinear error dynamics around the reference trajectory and design controller to drive the error to zero (see e.g. Frazzoli, Dahleh, & Feron, 2000; Kaminer, Pascoal, Hallberg, & Silvestre, 1998; Raptis & Valavanis, 2011; Raptis, Valavanis, & Moreno, 2011). In the latter approach, however, less experimental results have been reported. For path following, the classical approaches aim at designing control law to eliminate the track and cross-track error along the path. This is done by closing the path following loop around the track velocity vector as well as cross track position error (see e.g. Conte, Duranti, & Merz, 2004; Hoffmann, Waslander, & Tomlin, 2008). Similar to the modern approaches in trajectory tracking, the alternative modern approach for path following involves construction of path-dependent error space to express the dynamics of the vehicle. The error vector comprises velocity errors as well as cross track distance error. To derive the error dynamics to zero, a variety of controller synthesis techniques such as Linear Parameter Varying (LPV) can be used (Cunha, Antunes, Gomes, & Silvestre, 2006).

2.3. Guidance and control architecture

From a non-linear dynamical system's standpoint, two basic guidance formulations exist (Milam, 2003; van Nieuwstadt, 1996): *One-degree of freedom* (1-DOF) and *two-degree of freedom* (2-DOF). In the former, trajectory generation and tracking are solved simultaneously as a single problem. In a 2-DOF design the trajectory is generated separately and then used as a reference for a path tracking controller. Fig. 1 gives an overview of the architecture of the 2-DOF autonomous guidance system used in the authors' work (Dadkhah & Mettler, 2011). A *Receding Horizon* (RH) trajectory optimization is used to compute a local trajectory based on the current vehicle state and an *Active Waypoint* (AWP) in the vicinity of the vehicle. The AWP is determined during each planning cycle based on information about the immediate environment and a cost-to-go function that captures the cost of the discarded part of the trajectory (see e.g. the spatial value function in Mettler et al., 2010). The reference path computed by the RH trajectory optimization is specified by a sequence of points with reference speeds.

The trajectory optimization in this approach can be performed using linear or nonlinear programming techniques (Murray et al.,

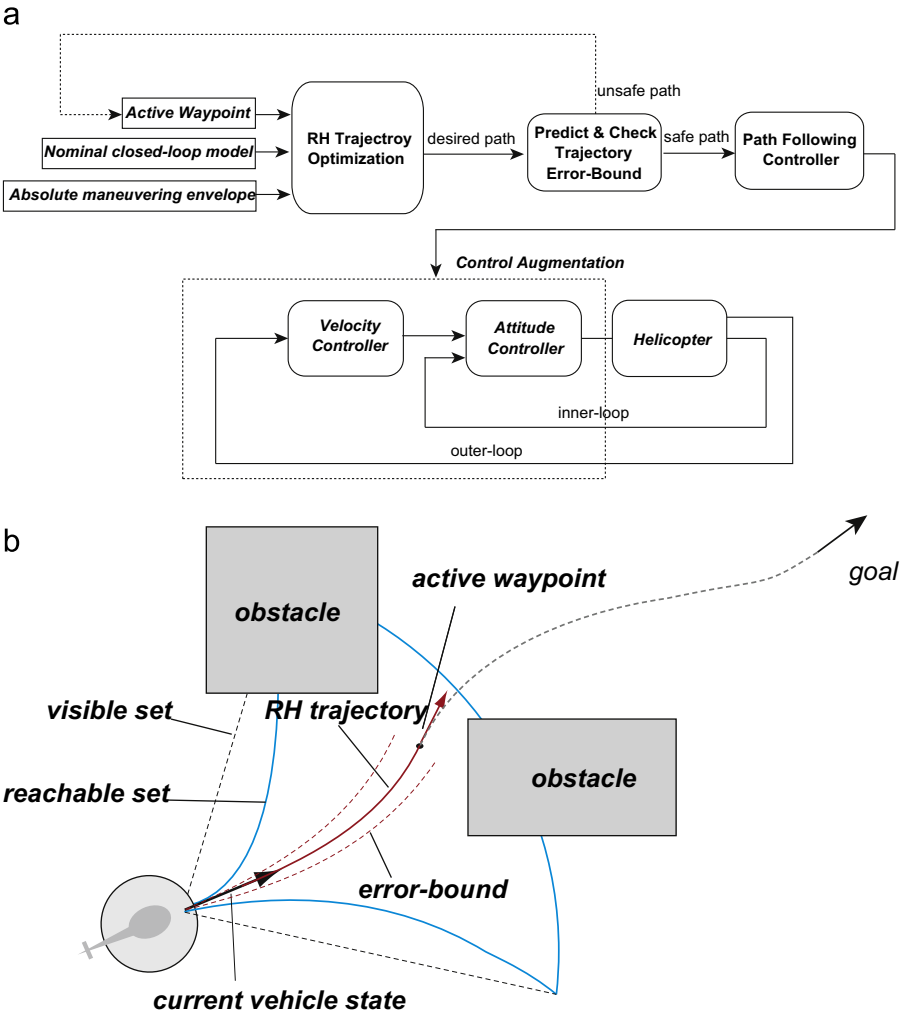

Fig. 1. (a) Overview of the path following controller as a part of the autonomous guidance system, (b) the figure shows the RH trajectory to the active waypoint (AWP) as well as the predicted error bound.

2003; Petit, Milam, & Murray, 2001). The dynamic models vary in their levels of details and fidelity. At the minimum, the model should describe a vehicle's absolute performance envelope as well as low-order, closed-loop dynamics. The closed-loop behavior describes the vehicles basic dynamic response characteristics. Accurate specification of the absolute maneuvering envelope is necessary to avoid generating infeasible trajectories for the closed-loop system. The maneuvering envelope is typically described by the maximum normal acceleration as a function of velocity. In addition, for operation in confined environments it is important to be able to predict the tracking error-bound in order to determine the safety of a candidate trajectory to the AWP. The tracking error is also often a function of the velocity. To summarize, the trajectory optimization must account for the following performance factors: (1) absolute maneuvering envelope; (2) nominal closed-loop model; and (3) trajectory error-bound for path following. All these factors are directly related to the closed-loop robustness and performance but require taking into account the effects of the path-following system and the basic nonlinearities in the vehicle dynamics.

2.4. Paper overview

The first part of the paper deals with rotorcraft dynamics and modeling, including the model uncertainties, and follows with the control design of a velocity tracking system based on a nested attitude-velocity design. μ analysis is applied to characterize the effects of the uncertainties on robustness and control performance. This system is then embedded within a path following architecture that regulates the cross track position error issuing velocity commands and feedforward attitude commands based on a closest point algorithm. The nonlinear vehicle dynamics are described by a point mass model. This allows accounting for the most important nonlinearities such as centrifugal forces arising when maneuvering. The second part of the paper introduces methods to evaluate the control system performance within the path-following architecture. First, experimental evaluation based on traditional time responses are provided that are then followed by an extension of the concepts of sensitivity and complementary sensitivity to the nonlinear dynamics.

3. Description of the helicopter test platform

The control and guidance technique are implemented and validated on a Blade-CX2 helicopter from E-flite. This helicopter has been used in various flight-test experiments conducted in the Interactive Guidance and Control Lab (IGCL), including human and autonomous guidance (Mettler, Dadkhah, Kong, & Andersh, 2013). This coaxial helicopter is one of the few commercially available miniature helicopter models in its size class that possesses all the significant functions of a full-sized helicopter. Lateral and longitudinal control is achieved through a conventional swash-plate mechanism, which produces cyclic blade pitch variation on the lower rotor. Fig. 2 shows the Blade-CX2 coaxial helicopter during flight experiment.

3.1. Airframe parametric model

For typical helicopters, the dynamics of the rotor system play an important role in the overall helicopter dynamics. The rotor is coupled to the fuselage dynamics via the effects of helicopter roll and pitch motion on the blade angle of attack and the inertial forces resulting from the fuselage angular rate. These effects are responsible for cross coupling between pitch and roll as well as attitude damping. The rotor system of the Blade-CX2 helicopter is

Fig. 2. Blade-CX2 helicopter during flight test in the Interactive Guidance and Control Lab (IGCL). The picture shows two of the Vicon tracking cameras, the control and Vicon tracking computers and RC transmitter.

similar to many other coaxial helicopter of this scale. It consists of a pair of co-axial, two-bladed rotors and a stabilizer-bar. The upper rotor receives the control augmentations from the stabilizer bar and the lower rotor receives the cyclic inputs from the swashplate. The two rotors are described in terms of first-order tip-path-plane (TPP) dynamics and are coupled to the fuselage translational and rotational dynamics via flapping force and moment derivatives. The top rotor equipped with a stabilizer bar is modeled as an equivalent TPP system where the time constant accounts for the damping effect of the stabilizer. The method follows the general approach described in Mettler (2002). The parametric model of the helicopter is given by an LTI system

$$\dot{x} = Ax + Bu$$
$$y = Cx \tag{1}$$

with state vector $x = [u, v, \theta, \phi, p, q, a, b, c, d]$ and control input $u = [u_{lon}, u_{lat}]$. The state-space matrices A, B and C are parametrized by the stability and control derivatives given in Appendix A.

The parametric model of the helicopter was identified using frequency-domain system identification techniques (CIFER Tischler & Cauffman, 1994). The identified parameters for the Blade-CX2 are given in Table 1 in Appendix A. A detailed account of the Blade-CX2 system identification is available in Dadkhah and Mettler (accepted for publication).

The servo actuators (E-flite S60) were identified in separate experiments. The frequency response was obtained by applying frequency sweep to the servo actuators through the labs ground station computer and custom electronics board. The response of the servo actuator was measured using the lab's Vicon motion tracking cameras. Fig. 3 shows the experimental frequency responses. Fig. 3 also shows the frequency response of the following actuator model obtained by fitting a first order transfer function with time-delay to the extracted frequency response

$$\frac{u_{out}}{u_{in}} = \frac{16.36}{s + 19.31} e^{-0.60s} \tag{2}$$

3.2. Modeling uncertainty

System identification techniques provide an estimate of the unknown parameters, along with the uncertainty in the identified parameters, in the form of error covariance or error percent. In the CIFER toolset (Tischler & Cauffman, 1994) used here, uncertainty percent is based on the Cramer–Rao bound. The Cramer–Rao

bound is determined from the diagonal elements of the inverse Hessian matrix associated with the cost function used in the identification of the parametric model based on the experimental frequency responses. The Cramer–Rao bound provides a lower bound on the identified parameter's standard deviation. As stated in Tischler and Remple (2006), a factor of 2 is needed to find a reasonable estimate of standard deviation:

$$CR_i = 2\sqrt{(H^{-1})_{ii}} \approx \sigma_i \tag{3}$$

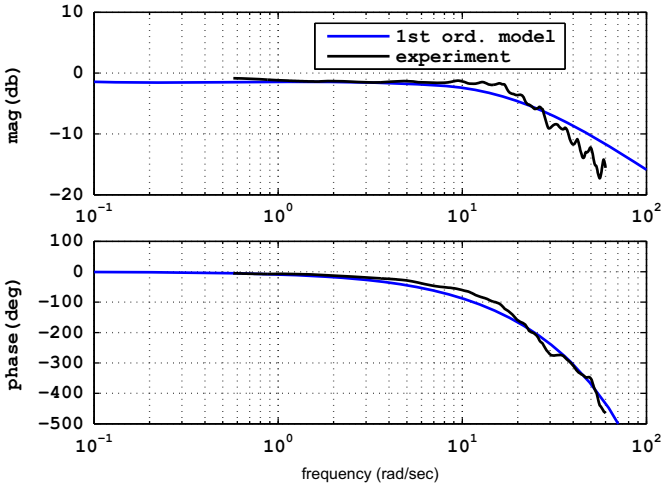

Fig. 3. Frequency response of actuator and the fitted 1st order transfer function.

CIFER's Cramer–Rao bound is used as an uncertainty measure for the identified stability derivative (shown in Table 1). This parametric uncertainty is modeled using Linear Fractional Transformation (LFT). Consider a nominal system given by M, the uncertainty in that system described by the Δ, the LFT gives the input–output of the model with its uncertainty as

$$y = F_u(M, \Delta) \tag{4}$$

$$y = (M_{22} + M_{21}\Delta_p(I - M_{11}\Delta_p)^{-1}M_{12})u \tag{5}$$

In addition to the parametric uncertainty, input multiplicative uncertainties are used to capture the actuator uncertainty and uncertainty in the cross coupling between lateral and longitudinal inputs. The LTI dynamic multiplicative uncertainty is given by

$$G_\Delta(j\omega) = G(j\omega)[I + W_m(j\omega)\Delta_i(j\omega)], \quad |\Delta_i(j\omega)| \le 1 \tag{6}$$

where ω is the frequency, $G(j\omega)$ is the nominal system and $W_m(j\omega)$ is the relative weighting function.

Fig. 4 illustrates the bode magnitude plot of the helicopter pitch and roll response to cyclic inputs. The plot includes the uncertain model along with the experimental frequency response data and the nominal identified model. The uncertain plant shown is generated using 20 random samples of the original uncertain plant. The results show that the experimental frequency responses are within the frequency response envelope resulting from the parametric and structured uncertainties. These frequency responses are used to analyze the robust stability and performance of the controller.

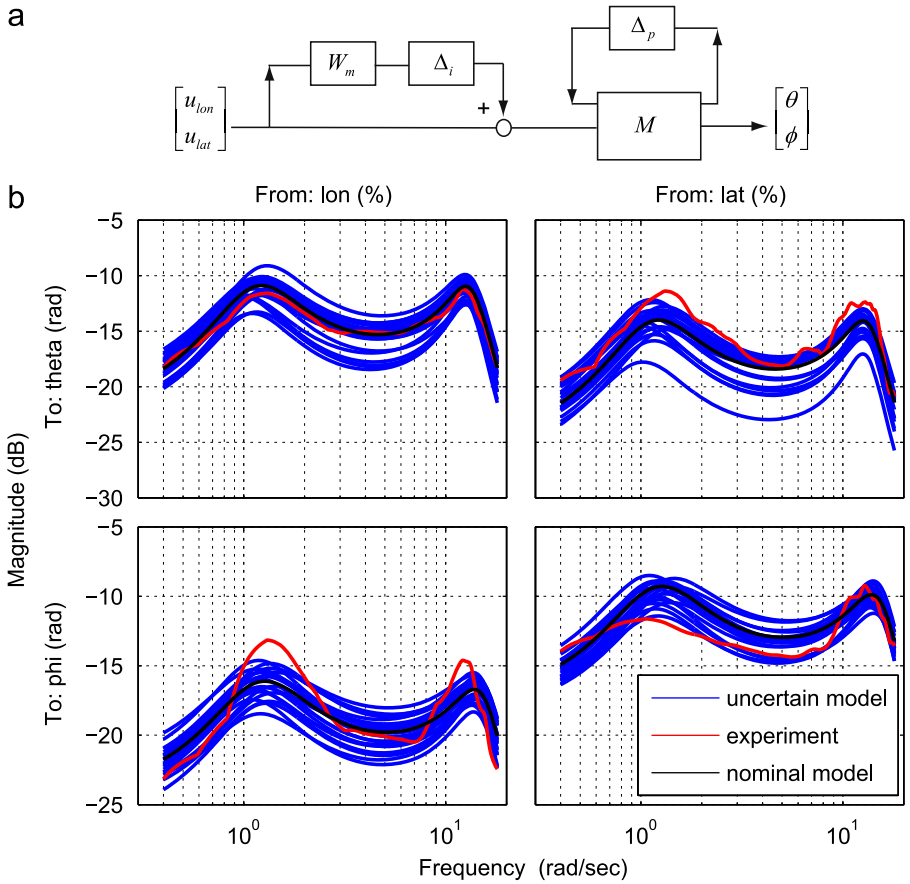

Fig. 4. Bode magnitude plot of the helicopter attitude dynamics (with inputs [u_{lon}, u_{lat}] and outputs [θ, ϕ]). The responses include the experimental frequency responses (red), the uncertain model (blue), and the response associated with the nominal identified model (black): (a) uncertainty model, (b) uncertain system frequency response. (For interpretation of the references to color in this figure caption, the reader is referred to the web version of this article.)

4. Control architecture

This section describes the architecture of the path following controller. The details are specific to the helicopter but the overall input–output response characteristics are common to other helicopter and rotorcraft. In helicopters, the cyclic blade pitch is used to control roll and pitch attitude (via the moments generated by the longitudinal and lateral tip-path-plane angles). The rotor thrust is approximately perpendicular to the TPP. Therefore, a change in attitude (superposed with TPP) acts as a form of thrust vectoring. The difference in time constants associated with the rotor and fuselage rotation and the fuselage translation are typically sufficiently large to allow the use of the attitude angle as a pseudo-control input for the translational motion.

A nested control architecture is common in helicopters and other rotorcraft. An attitude inner-loop provides fast and accurate pitch and roll response. A velocity outer-loop uses the attitude angles as pseudo-control inputs to control the propulsive longitudinal and lateral forces. A classical loop-shaping technique is used for the inner-loop frequency responses. For the outer velocity loop a dynamic inversion technique is used. The desired dynamics are based on the reduced-order velocity-attitude dynamics of the helicopter. Fig. 5 shows the block diagram of the nested velocity-attitude control loop architecture. The design of the attitude and velocity controllers as well as robustness analysis are explained in detail in Sections 4.1 and 4.2, respectively. Section 4.3 describes how the velocity control system is incorporated within the path following system to enable required tracking performance.

4.1. Attitude controller

The inner-loop is an attitude controller that relies on pitch and roll feedback measurements. Angular rate damping is provided mechanically by the helicopter's top rotor and stabilizer bar. Fig. 6 shows the experimental frequency responses for the attitude dynamics. As can be seen, for the Blade-CX2 helicopter, the Phugoid mode is lightly damped in comparison to other miniature helicopter (e.g. the R-50 Mettler et al., 2000 or the X-Cell Mettler, Dever, & Feron, 2004). The same observation can be made about the coupled Fuselage-Rotor-Stabilizer bar (FRS) mode. Finally, the pseudo-rate feedback provided by the stabilizer-bar generates enough phase lead that a PD or lead type compensator is not required.

With a nested velocity control architecture it is important for the inner attitude control loop to have the highest possible bandwidth (BW). The BW of the velocity loop should not be higher than about half the attitude loop BW to ensure sufficient time-scale separation between the two loops. One way to slow down the attitude control system is to avoid including integral action in that loop. Ultimately, however, the BW is limited by the natural frequency of the FRS mode as well as the time-delay. According to Skogestad and Postlethwaite(2005), it is recommended to limit the crossover frequency ω_c of the system to

$$\omega_c < 1/\theta_d \tag{7}$$

where θ_d is the time delay. Given the approximate $\theta_d = 60$ ms delay in the experimental setup, the bandwidth is limited to about 16 rad/s.

The lightly damped FRS mode in the attitude dynamics can be compensated by a second order notch filter matching the damping and natural frequency of the FRS mode in each axis (Mettler et al., 2000)

$$N(\zeta,\omega) = \frac{s^2 + 2\zeta\omega s + \omega^2}{s^2 + 2\omega s + \omega^2} \tag{8}$$

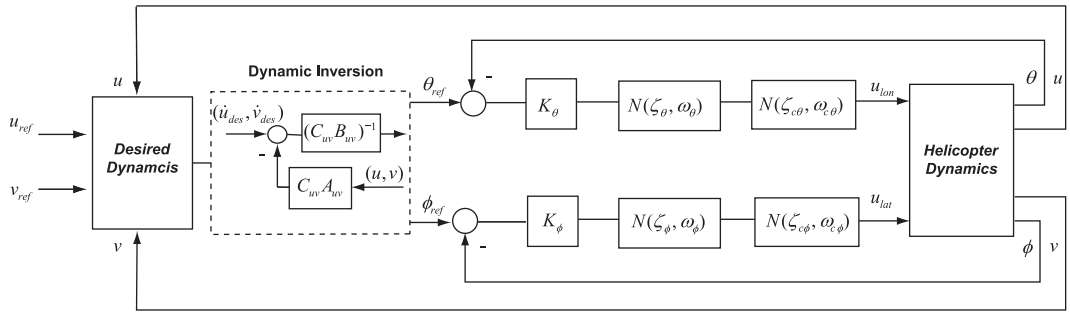

Fig. 5. Nested velocity control architecture.

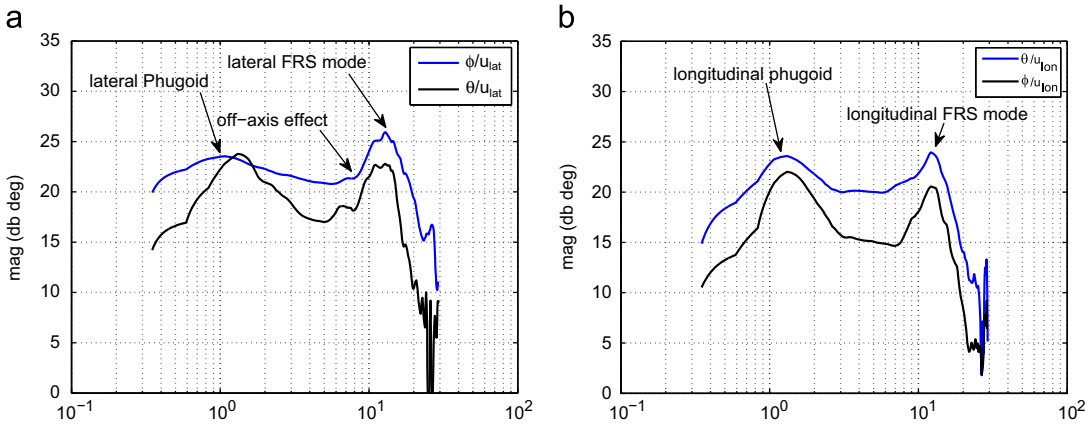

Fig. 6. Experimental attitude frequency responses highlighting the lightly damped lateral and longitudinal Fuselage-Rotor-Stabilizerbar (FRS) modes as well as the lightly damped Phugoid mode.

with

$$\omega_\theta = 12.35 \text{ rad/s}, \quad \zeta_\theta = 0.2$$
$$\omega_\phi = 12.86 \text{ rad/s}, \quad \zeta_\phi = 0.2 \tag{9}$$

As can be seen from Fig. 6, for the Blade-CX2 helicopter, the off-axis RFS mode has a frequency very close to the on-axis FRS mode. Therefore, the above notch filters are capable of eliminating the coupling. However, some off-axis effects are observed around the frequency of 8 rad/s. To remove the effect of this coupling a notch filter is inserted in the off-axis loop. The parameters of the notch filter are

$$(\omega_{c\theta}, \zeta_{c\theta}) = (\omega_{c\phi}, \zeta_{c\phi}) = (8, 0.4) \tag{10}$$

The gains K_θ, K_ϕ in the block diagram depicted in Fig. 5 are used to adjust the BW. The maximum BW is determined based on the minimum amount of phase-margin (PM) and gain-margin (GM) needed to achieve sufficient robustness. With the following set of gains:

$$K_\theta = -0.1180\%/\text{deg}$$
$$K_\phi = 0.106\%/\text{deg} \tag{11}$$

The attitude controller achieves a bandwidth between about 4–5 rad/s with 100 deg of PM and/or 12 db of GM.

Fig. 7 shows the resulting loop-shapes along with the controller and open-loop frequency responses. Notice from the loop-gains that the bandwidth could still be increased using larger feedback gains (K_θ, K_ϕ). The available PM comes from the pseudo-rate feedback effect of the stabilizer-bar. However, this would be detrimental for the GM as the GM of less than 10 db would compromise robustness.

The robust stability and robust performance of the attitude control system with respect to the modeling uncertainties shown in Fig. 4, which were discussed in Section 3.2, is evaluated using μ analysis (Balas, Chiang, Packard, & Safonov, 2005). The results are shown in Fig. 8. In regard to robust stability, the μ analysis reveals that the attitude controller has a μ value less than one across all frequencies. This means that the inner-loop is robustly stable with respect to the given parametric and structured uncertainties. On the other hand, in regard to robust performance, the μ analysis shows a μ value greater than unity. The velocity controller therefore will not achieve robust performance.

4.2. Velocity controller

The velocity control system follows a nested loop design where the pseudo-control (the attitude angles) is determined from a dynamic inversion. The nested control architecture is based on the time-scale separation between the high frequency and low frequency modes. The low-frequency dynamics are the fuselage translational dynamics with states $[u, v, \theta, \phi]$. The high-frequency ones correspond to the attitude fuselage dynamics coupled with the rotor tip-path-plane dynamics with states $[p, q, a, b, c, d]$. According to the helicopter dynamics given in (37), the dynamics governing the translational states are

$$\dot{u} = X_u u + X_\theta \theta \tag{12}$$

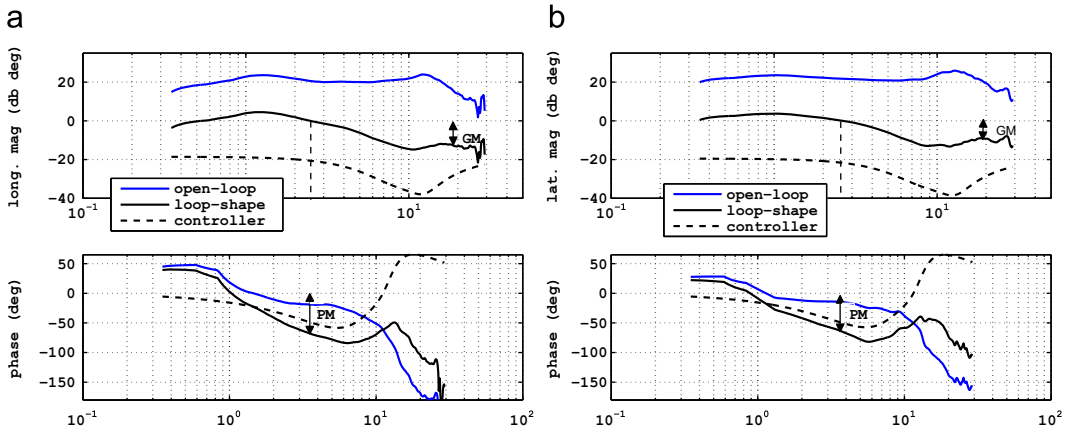

Fig. 7. Loop shapes obtained using a classic loop-shaping procedure. Notice how the notch filter eliminates the FRS coupling and ensures that a sufficient phase margin is achieved: (a) longitudinal, (b) lateral.

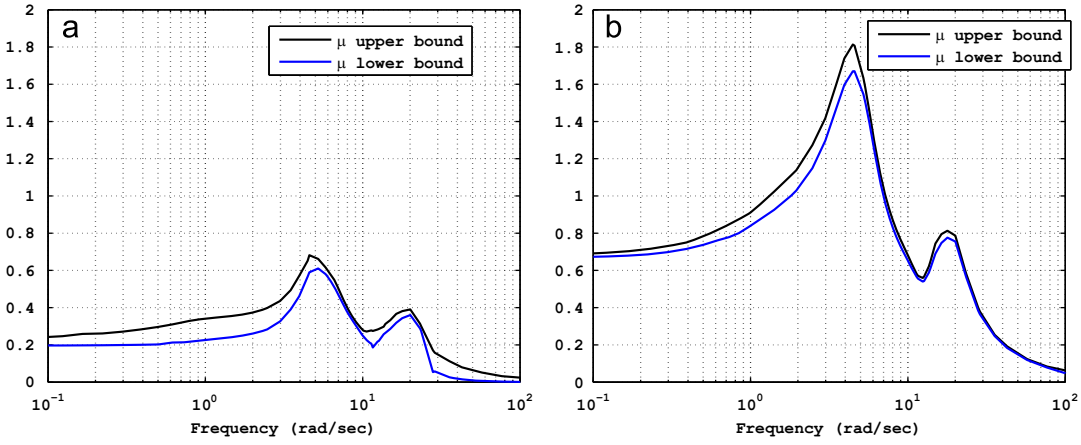

Fig. 8. Result of the μ analysis for the attitude controller: (a) μ for robust stability, (b) μ for robust performance.

$$\dot{v} = Y_v v + Y_\theta \theta \tag{13}$$

This system can be written in the following state-space form:

$$\frac{d}{dt}\begin{bmatrix} u \\ v \end{bmatrix} = A_{uv}\begin{bmatrix} u \\ v \end{bmatrix} + B_{uv}\begin{bmatrix} \theta \\ \phi \end{bmatrix} \tag{14}$$

where here $[u, v]$ are the Controlled Variable (CV) (Anon, 1996). The basic dynamic inversion equation for computing attitude commands is

$$\begin{bmatrix} \theta \\ \phi \end{bmatrix}_{ref} = (C_{uv}B_{uv})^{-1}\left(\begin{bmatrix} \dot{u} \\ \dot{v} \end{bmatrix}_{des} - C_{uv}A_{uv}\begin{bmatrix} u \\ v \end{bmatrix}\right) \tag{15}$$

where C_{uv} is the identity matrix ($I_{2\times 2}$). The "desired dynamics" are determined using feedback from the CV as well as the reference velocity. In general these are composed of a PI-term combined with a feedforward term (Enns & Keviczky, 2006)

$$\frac{dCV_{des}}{dt} = K_f\frac{dCV_{cmd}}{dt} + K_b(f_c CV_{cmd} - CV + z) \tag{16}$$

$$\frac{dz}{dt} = f_i K_b(CV_{cmd} - CV) \tag{17}$$

The proportional gain K_b sets the bandwidth, the integral gain f_i is used for desensitization and disturbance rejection, and the command gain f_c is used to achieve the desired command response. The feedforward gain K_f was not used here. A pre-filter can also be included to smooth the command signal. Fig. 9 shows the block diagram for the "desired dynamics". The controller gains used for the experimental implementation are

$$f_c = 1, \quad f_i = 0.01, \quad K_b = 2 \tag{18}$$

The resulting closed-loop is

$$\frac{K_b(f_c s + f_i K_b)}{s^2 + K_b s + f_i K_B^2} = \frac{2(s + 0.02)}{s^2 + 2s0.04}. \tag{19}$$

The μ analysis for robust stability against the parametric and structured uncertainty indicates that the velocity controller achieves a μ value less than one over the entire frequency range (see Fig. 10). The robust performance μ analysis, however, shows that the velocity controller results in a μ value greater than one. The velocity controller therefore will not achieve robust performance. Although a higher level of performance might be expected for the Blade-CX2 helicopter, the achievable performance is limited by several factors including the time-delay (around 60 ms) associated with the experimental setup; the relatively low bandwidth actuators (around 12 rad/s); and the powerful tuning of the stabilizer-bar. All these factors contribute in making it difficult to achieve robust performance. It is important to keep in mind that helicopters like the Blade-CX2 are hobby helicopter that were developed primarily for indoor flight and stable enough to allow operation by inexperienced pilots.

4.3. Path following control architecture

As explained in Section 2 the receding horizon trajectory optimization provides a reference path over a finite horizon. The reference path is specified by a set of waypoints and velocity vectors (p_i, v_i), $i = 1, \ldots, H$ given in inertial frame. For a rigid-body system, such a reference path cannot be adequately tracked by linear velocity control systems. The nonlinear effects that are associated with the rigid-body motion need to be accounted for. The path following problem can be analyzed using a simplified mass-point model of the helicopter dynamics (see Appendices B and C). This model abstracts out the details of the rotor dynamics. This simplification is possible thanks to the control augmentation provided by the attitude and velocity control loops.

The primary nonlinear effects occurring in rigid-body motion are the normal acceleration arising in the presence of path curvature $a_n = V^2/\rho$. The analysis given in the Appendix shows

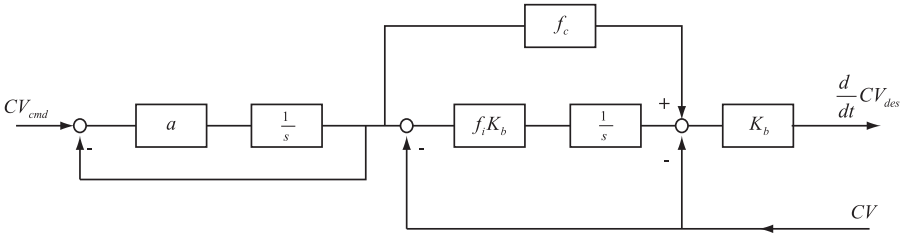

Fig. 9. Desired dynamics for dynamic inversion controller.

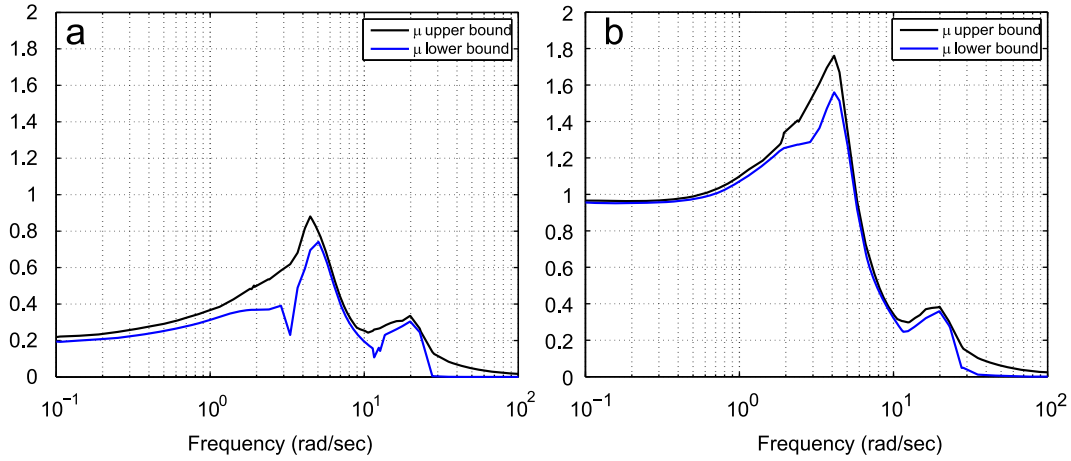

Fig. 10. Result of the μ analysis of the velocity control system: (a) μ upper bound for robust stability, (b) μ upper bound for robust performance.

that the radial and tangential (so-called cross-track and track) error can be adequately regulated by two decoupled PD controllers.

Fig. 11 shows the path following tracking architecture derived from the mass-point analysis. The error between the current helicopter position and velocity and the reference waypoints and velocities is parameterized in terms of cross-track error. This error and the reference velocity are transformed into body coordinates. The body-frame velocity reference is applied to the velocity controller. The normal error vector, which is in the direction of centrifugal acceleration, is passed through a PD element and applied as feedforward command signal for the attitude controller. The feedforward guarantees that an adequate amount of thrust is generated in the direction normal to the path to generate the normal acceleration required to track the specified curvature.

The remainder of this section describes the *Closest-Point Algorithm* (based on Conte et al., 2004). A continuous spline description of the path is computed by fitting a cubic spline to the sequence of waypoints. The latter can be described as a parametrically in terms of the path arc length s:

$$p(s) = as^3 + bs^2 + cs + d, \tag{20}$$

where s is obtained by linear approximation of the path length between two subsequent waypoints p_i and p_{i-1}:

$$s_i = s_{i-1} + \|p_i(s) - p_{i-1}(s)\| \tag{21}$$

The vectors a, b, c and d are then computed via a cubic spline interpolation algorithm (see e.g. Press, Teukolsky, Vetterling, & Flannery, 2002). A spline description of the path is used to determine the tangent and normal to the path and helps deal with possible discontinuities. For each value of s the tangent $t(s)$ and normal $n(s)$ vectors are obtained as follows:

$$\begin{aligned} t(s) &= 3as^2 + 2bs + c \\ n(s) &= t \times q \times t/|t^4| \\ q(s) &= 6as + 2b \end{aligned} \tag{22}$$

Given the helicopter position in inertial frame, the closest reference point s^* on the path is obtained knowing that the error vector from the vehicle position to the reference point e has to be normal to the tangent vector

$$e_t(s) = e(s) \cdot \frac{t(s)}{\|t(s)\|} \tag{23}$$

where $e(s) = p(s) - [x, y]^T$ (see Fig. 12). To find the reference point that satisfies this condition, the following recursive equation can be used (Conte et al., 2004):

$$s_n = s_{n-1} + \frac{e_t(s_{n-1})}{\|t(s_{n-1})\|} \tag{24}$$

The closest reference point $s^\star$ is then used to compute the cross-track error vector ${}^I e_n(s^\star)$ and the desired tangent velocity vector ${}^I v_t(s^\star)$ (the superscript I stands for inertial frame). These vectors are then transformed into the helicopter body frame B using the rotation matrix $C_I^B(\psi)$:

$$\begin{bmatrix} {}^{\mathrm{I}} e_n(s^\star) \\ {}^{\mathrm{I}} v_t(s^\star) \end{bmatrix} = C_I^B(\psi) \begin{bmatrix} {}^{\mathrm{B}} e_n(s^\star) \\ {}^{\mathrm{B}} v_t(s^\star) \end{bmatrix} \tag{25}$$

where ψ is the body frame heading angle. Finally these signals are incorporated into the control system as illustrated in Fig. 11.

4.4. Path following design and control design summary

Constant gains were used (nominal speed for the design is $v_0 = 0.5$ m/s). The normal and tangential accelerations are generated via the helicopter attitude. For small attitude angles, the rotor thrust is approximately equal to the total weight and therefore the horizontal acceleration is simply the product of the attitude and the gravitational acceleration. The lateral PD gains are $K_{p,y} = 0.26$ rad/m and $K_{d,y} = 0.035$ rad/m/s. For the longitudinal direction identical gains were used ($K_{p,x} = -0.26$ rad/s and $K_{d,x} = -0.035$ rad/m/s).

The attitude control system represents the core component and acts as the actuation system used to generate the normal and tangential accelerations. The path following system is responsible for tracking the curvature and speed through the normal and tangential accelerations. The former is implemented using the PD feedforward and the latter using the dynamic inverse velocity controller.

In summary, the overall control system design as follows:

1. The first step consists in the design of the attitude control system. The design objective is to achieve the highest bandwidth given the limitations set by the coupled rotor-fuselage mode and time delays in the system. Loop shaping provides the essential design framework for this system. The attitude tracking performance can be determined from robust control analysis and flight testing (Fig. 13). The attitude control system

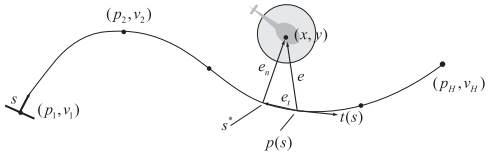

Fig. 12. Illustration of closest point computation.

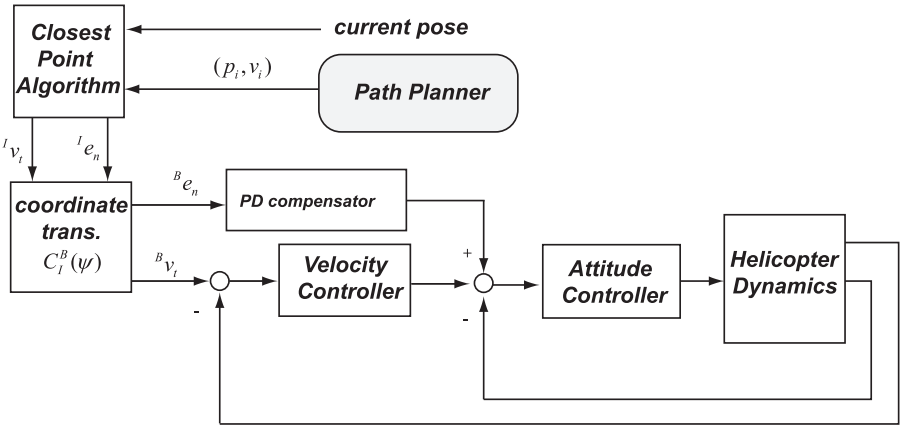

Fig. 11. Path following controller architecture.

achieves a BW of about 4–5 dB for both roll and pitch with a settling time of about 0.5 s.

2. The second step consists in the design of the velocity control system. This system is based on the dynamic inverse design framework. The main parameters are the desired dynamic model. Integral action is required to provide adequate command tracking. The proportional gain determines the bandwidth. The BW of the velocity control system must be about half that of the attitude control system to guarantee sufficient separation. The velocity control system is tested using the typical step responses (Fig. 14). These results show a settling time of about 1.3 s. As will be described in the next section, more comprehensive testing is performed using the generalized sensitivity and complementary sensitivity functions (31) on the circle test data in Fig. 19. As can be seen from Fig. 18, the velocity control system achieves a BW between about 1–3 dB, which is consistent with the settling time obtained from the step-response experiments.
3. The final step is the integration under the path following controller. The path following addresses the control issues that arise from the nonlinear path following dynamics. The three components of this system include the closest-point algorithm, the coordinate transforms and the PD feedforward element (see Fig. 11). The parameters of the PD are set based on the attitude and velocity control performance. As will be described in the following section, the performance of the overall path tracking system is evaluated using circular trajectories at different speed and curvatures. The results are shown in Fig. 20.

The design procedure highlights how the design requirements for the different components determine their integration and the overall system performance. The following section describes the performance evaluation of the overall system.

5. Experimental evaluation

Autonomous guidance calls for control performance requirements that are not fully captured by traditional robust control methods or the traditional handling qualities metrics. This section provides experimental evaluation of the control system as well as the description of the performance requirements called for by the autonomous guidance system that was described in Section 2. The testing and evaluation approach considers the closed-loop system and therefore can in principle be applied to any particular rotorcraft and control augmentation. First the experimental facility is briefly described. It is then followed by a traditional evaluation of the attitude and velocity control laws and subsequently the evaluation focusing on the path following performance characteristics including its absolute maneuvering envelope and the path tracking error characteristics.

5.1. Experimental facility

The controller was implemented and evaluated in the Interactive Guidance and Control Lab (IGCL) (see Mettler et al., to appear

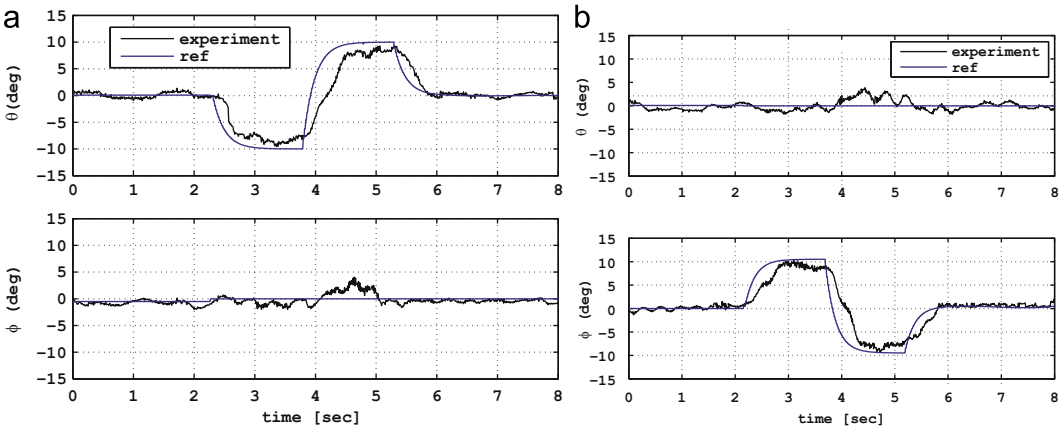

Fig. 13. Flight test results for the attitude controller: (a) longitudinal doublet, (b) lateral doublet.

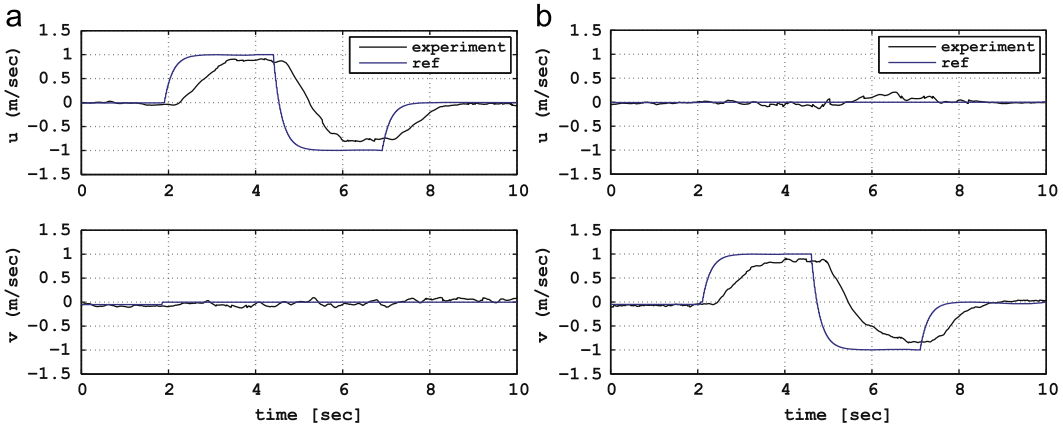

Fig. 14. Flight test results for velocity controller: (a) longitudinal doublet, (b) lateral doublet.

for details). The vehicle's 6-DOF data is provided in real time by Vicon MX motion tracking cameras, eliminating the need for onboard navigation sensors. The control software is written in C++ and integrated with a motion capture system and other components of the lab environment using the Robotics Operating System (ROS) (Quigley et al., 2009). ROS is an open-source meta-operating system, which provides tools and libraries as well as services such as message-passing between processes, package management, and low-level device control.

The implementation using the Vicon tracking cameras and ground computer involves greater time delays than typical onboard implementation or manual RC control (Mettler et al., 2010).

5.2. Evaluation of the velocity and attitude controllers

The performance of the velocity and attitude controllers is evaluated by applying doublet reference signals. The controllers are implemented and run at 100 Hz. However, due to limitations of the RC transmitter, the control signals are sent to the helicopter at 50 Hz. The controllers were discretized using a used zero-order hold (ZOH) transformation.

The inner-loop attitude controller was evaluated by applying a doublet reference of 10 deg magnitude and 1.5 s pulse duration. The tracking performance of the velocity control system was evaluated by applying a doublet velocity command of 1 m/s magnitude and 2 s pulse duration. Fig. 13 shows the tracking performance of the inner-loop and Fig. 14 shows the tracking performance of the velocity controller.

5.3. Evaluating closed-loop absolute maneuvering envelope

Characterizing the absolute maneuvering envelope for the closed-loop system is necessary to ensure that the closed-loop model used by the trajectory planner is accurate and does not generate infeasible trajectories. The values of normal acceleration that the helicopter can sustain determine the upper-bound on the maximum curvature. Based on the centrifugal effects, for the same normal acceleration, a higher curvature can be achieved at lower velocity magnitude and vice versa. The absolute limit in normal acceleration depends on the maximum attitude and thrust that can be sustained. The curvature-velocity plot is a convenient way to depict the maneuvering envelope since it has a geometric interpretation (Spenko, Kuroda, Dubowsky, & Iagnemma, 2006).

Consider a general helicopter trajectory as shown in Fig. 15 where v_t and a are total horizontal velocity and acceleration vectors in inertial frame, respectively. The normal acceleration a_n and curvature of the path can be computed from

$$\|a_n\| = \|a\|\sin(\xi) \tag{26}$$

$$\kappa = \frac{\|a_n\|}{\|v_t\|^2} \tag{27}$$

where ξ is the angle made by the velocity and acceleration vectors

$$\xi = \sin^{-1}\frac{a \times v_t}{\|a\|.\|v_t\|}. \tag{28}$$

The upper bound on curvature-velocity curve can be computed from the maximum roll angle ϕ_{max} for the bare airframe and using the assumption that the helicopter stays level altitude. The thrust is given by $T = mg/\cos(\phi_{max})$. The maximum acceleration based on the normal acceleration is given by

$$a_{max} = g\tan(\phi_{max}) \tag{29}$$

where g is the gravitational acceleration. Hence, the following relation provides the upper-bound for the curvature-velocity space

$$\kappa = \frac{g\tan(\phi_{max})}{\|v_t\|^2} \tag{30}$$

Fig. 16(a) shows the curvature-velocity characteristic of the Blade-CX2 helicopter under closed-loop velocity control in a free-flight task. The experiment was conducted in the lab environment. The velocity commands were generated by the pilot via a joystick. The red line shows the upper-bound (30). The black dots show the curvature-velocity points for 12 experiments used for the tracking performance evaluation. In addition, Fig. 16(b) shows the normal and tangential acceleration of the vehicle during the same flight and the corresponding upper bound. The data for the plots were computed using (28) to (27).

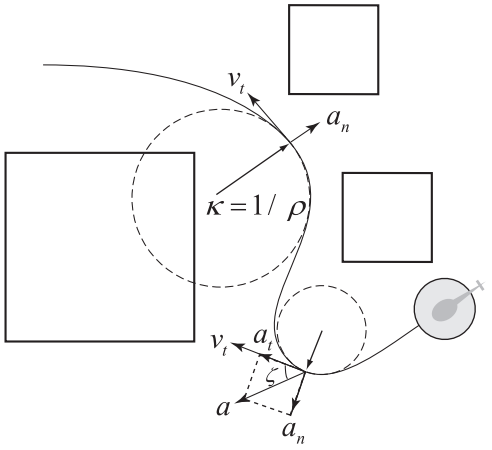

Fig. 15. Parametrization of a general trajectory amid obstacles.

5.4. Performance and robustness analysis of the velocity controller

Traditional performance and robustness analysis relies primarily on the sensitivity $|S(j\omega)|$ and complementary sensitivity functions $|T(j\omega)|$. The sensitivity function describes the behavior of the tracking error e. The complementary sensitivity function describes how a measurement noise n affects the output y. However, if the closed-loop system contains nonlinearities, the frequency responses for $|S(j\omega)|$ and $|T(j\omega)|$ cannot be interpreted in this traditional manner.

The notion of a steady-state response to harmonic excitation is undefined for general nonlinear systems because such systems can have multiple coexisting periodic and even chaotic responses to a harmonic excitation. However, for the special class of so-called convergent nonlinear systems any bounded input produces a uniformly bounded, globally asymptotic stable solution (Pavlov, Wouw, & Nijmeijer, 2007) (which is called a steady-state solution). The convergence property can usually be achieved through a feedback controller.

Suppose that the helicopter closed-loop velocity control system is uniformly convergent. Then the *generalized sensitivity and complementary sensitivity functions* are defined as follows:

$$S(v,\omega) = \frac{\|e_{v\omega}\|_2}{\|r_{v\omega}\|_2}, \quad T(v,\omega) = \frac{\|y_{v\omega}\|_2}{\|r_{v\omega}\|_2} \tag{31}$$

where v is the harmonic excitation magnitude and ω is its frequency (Pavlov, van de Wouw, Pogromsky, Heertjes, & Nijmeijer, 2007). Notice that due to nonlinearity of the system, $S(v,\omega)$ and $T(v,\omega)$ depend not only on the excitation frequency ω but also on

the amplitude v. In addition, for MIMO systems the frequency responses also depend on the direction of the input signal. Therefore, the *generalized sensitivity and complementary sensitivity functions* for MIMO systems can be define as follows:

$$S(v,\omega)=\max_{r_{v\omega}\neq 0}\frac{\|e_{v\omega}\|_2}{\|r_{v\omega}\|_2},\quad T(v,\omega)=\max_{r_{v\omega}\neq 0}\frac{\|y_{v\omega}\|_2}{\|r_{v\omega}\|_2} \tag{32}$$

By choosing the velocity reference signal $r_{a\omega}$ for the velocity control system as

$$r_{a\omega}=\begin{bmatrix} a\cos(\omega t)\\ a\sin(\omega t)\end{bmatrix} \tag{33}$$

one can find the maximum gain for $S(a,\omega)$ and $T(a,\omega)$ according to Eq. (32) as the direction of input vector is varied for the given input magnitude a and frequency ω.

By varying the frequency and magnitude of the reference command it is possible to evaluate the trajectory tracking performance around a particular equilibrium trajectory. Given the space constraints in the IGCL's indoor facility it is not possible to evaluate the tracking performance for the full range of operating points. Nevertheless, it is possible to sample the curvature-velocity diagram (see points on Fig. 16(a)) by following circular trajectories and holding the heading constant. The reference command $r_{v\omega}$ in Eq. (33) corresponds to the circular trajectory with constant heading as shown in Fig. 17. The radius of the trajectory can be obtained via $R=v/\omega$.

Fig. 19 shows the experimental tracking performance when applying the velocity reference command of Eq. (33) for different magnitudes and frequencies corresponding to the 12 experimental curvature-velocity points shown in Fig. 16a. Note that due to the space limitation, the frequencies are constrained to lie between 0.35 rad/s and 3.5 rad/s. As can be seen in Fig. 19, the executed circular trajectories are drifting over time due to noise and disturbances. These flight tests were used to compute the generalized sensitivity and complementary sensitivity function of the overall velocity control system at different input magnitudes and frequencies according to Eq. (32). Fig. 18 shows the comparison between the sensitivity and complementary sensitivity function of the nominal linear model and the ones obtained applying this procedure.

5.5. Performance evaluation of path following system

The flight test results for the same 12 test points with the path following system are depicted in Fig. 20. Compared to Fig. 19, where the path following loop is not active, no drift in the trajectories is visible. The small deviations in tracking are due to the effects of disturbances and the input–output characteristics of

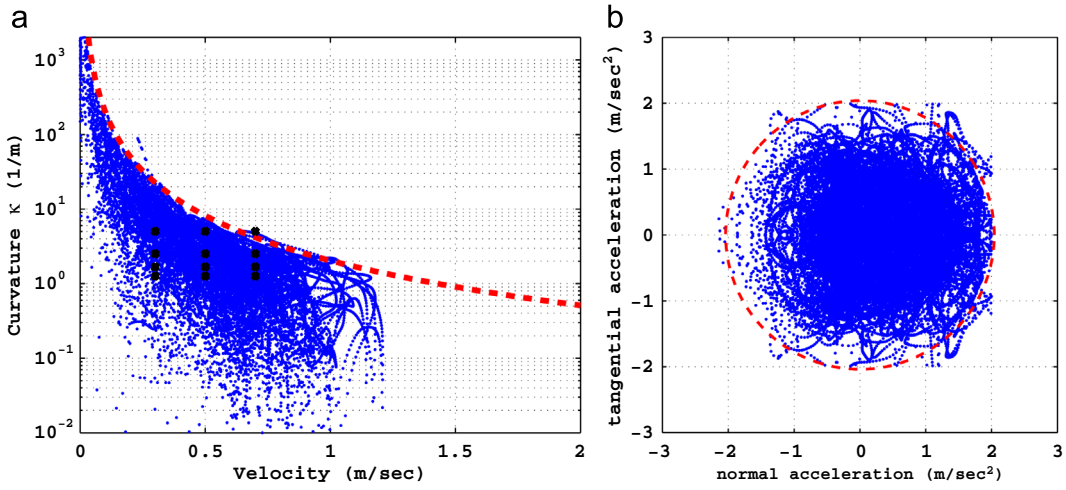

Fig. 16. (a) Curvature-velocity plot obtained for the Blade-CX2 helicopter in closed-loop: the curvature-velocity points are constrained by the absolute total acceleration limit (red line). The black dots are the curvature-velocity coordinates for the path tracking experiments. (b) Normal and tangential acceleration characteristics of the Blade-CX2 helicopter in closed-loop. (For interpretation of the references to color in this figure caption, the reader is referred to the web version of this article.)

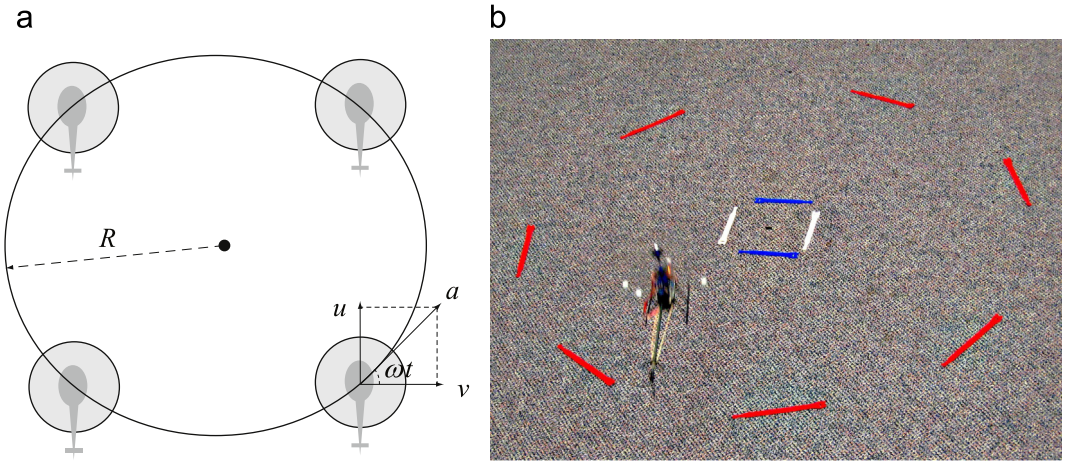

Fig. 17. Circular trajectory with constant heading, which corresponds to applying the reference command of Eq. (33) to the velocity control system.

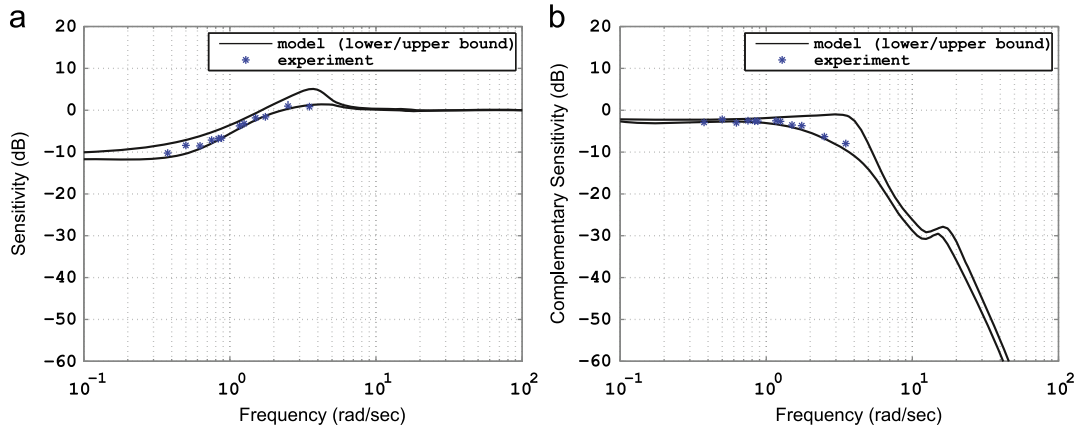

Fig. 18. Sensitivity and complementary sensitivity functions obtained from the linear model as well as experimental data obtained from the circle tests at different velocities and frequencies: (a) sensitivity, (b) complementary sensitivity.

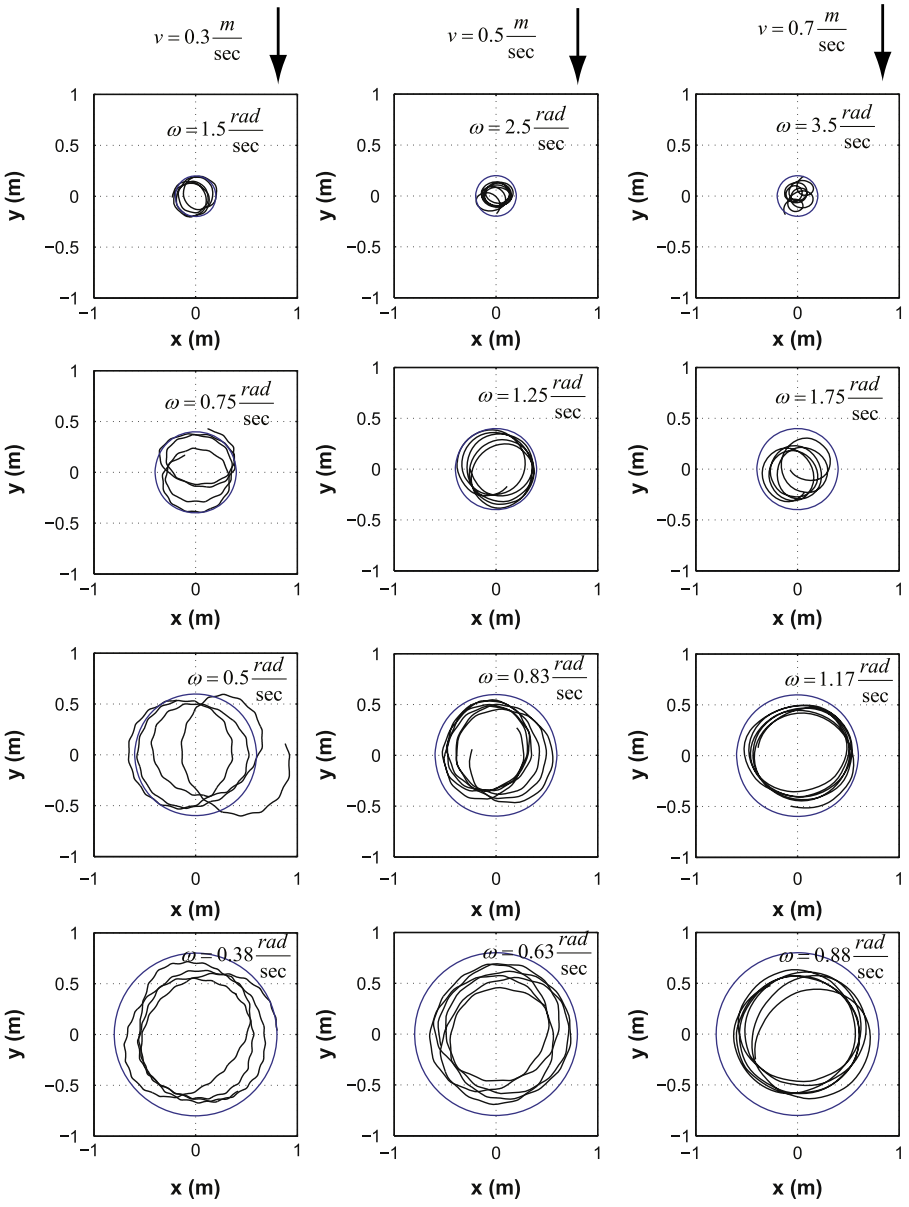

Fig. 19. Experimental tracking performance based on circular trajectories obtained by applying the reference velocity commands of Eq. (33) with different magnitude and frequency corresponding to the 12 test points in Fig. 16(a).

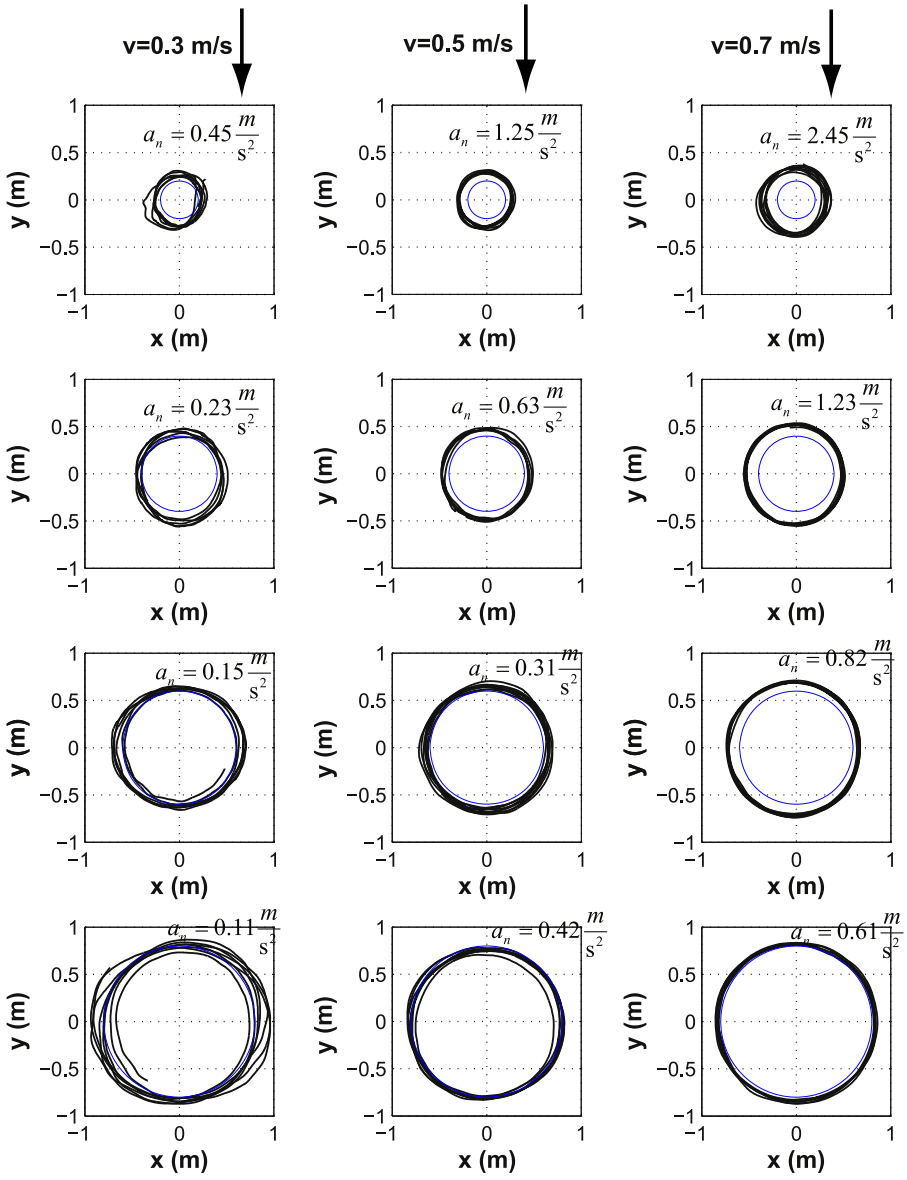

Fig. 20. Experimental tracking performance of the path following controller for the same conditions as in Fig. 19.

the closed-loop system. To further characterize the tracking performance the flight data is used to generate histograms of the tracking error (see Fig. 21). The mean and variance of the tracking error are modeled by fitting each histogram using Gaussian density functions. These values are depicted as a function of velocity and normal acceleration in Fig. 22. Linear interpolation was used to cover the entire velocity and normal acceleration range. From these plots it is clearly visible that tracking error is primarily a function of normal acceleration with a much smaller small speed effect.

5.6. Tracking error model

To ensure safe operation when operating amidst obstacles, it is critical to be able to predict the tracking error bound (see Fig. 23). The goal therefore is to determine a tracking error model that can be used in real-time to predict the tracking error bound based on a pre-specified path generated by a path planner. Fig. 24 shows the block-diagram of error prediction model.

The error model is based on a simplified first-order model of the inner-loop. Un-modeled effects and modeling uncertainties and disturbances are described by noise parameters η_x and η_y. According to the bock-diagram in Fig. 24, the differential equation governing the path tracking dynamics are as follows:

$$\begin{aligned}
\theta_{ref} &= X_\theta^{-1}[\dot{u}_{des} - X_u u] \\
\phi_{ref} &= Y_\phi^{-1}[\dot{v}_{des} - Y_v v] \\
\dot{\theta} &= -1/\tau\theta + 1/\tau\theta_{ref} + K_p e_x + K_d \dot{e}_x + \eta_x \\
\dot{\phi} &= -1/\tau\phi + 1/\tau\phi_{ref} + K_p e_y + K_d \dot{e}_x + \eta_y \\
\dot{u} &= X_u u + X_\theta \theta \\
\dot{v} &= Y_v v + Y_\phi \phi \\
\dot{x} &= u \\
\dot{y} &= v
\end{aligned} \tag{34}$$

where $e = [e_x, e_y]$ is the normal tracking error vector which is computed according to the *closed-point algorithms* in Section 4.3.

The noise parameters η_x and η_y are zero-mean Gaussian random variables. They are determined by matching the predicted error statistics with those obtained from the experiments. The gains K_p and K_d are the path following controller's PD gains. Fig. 25 shows

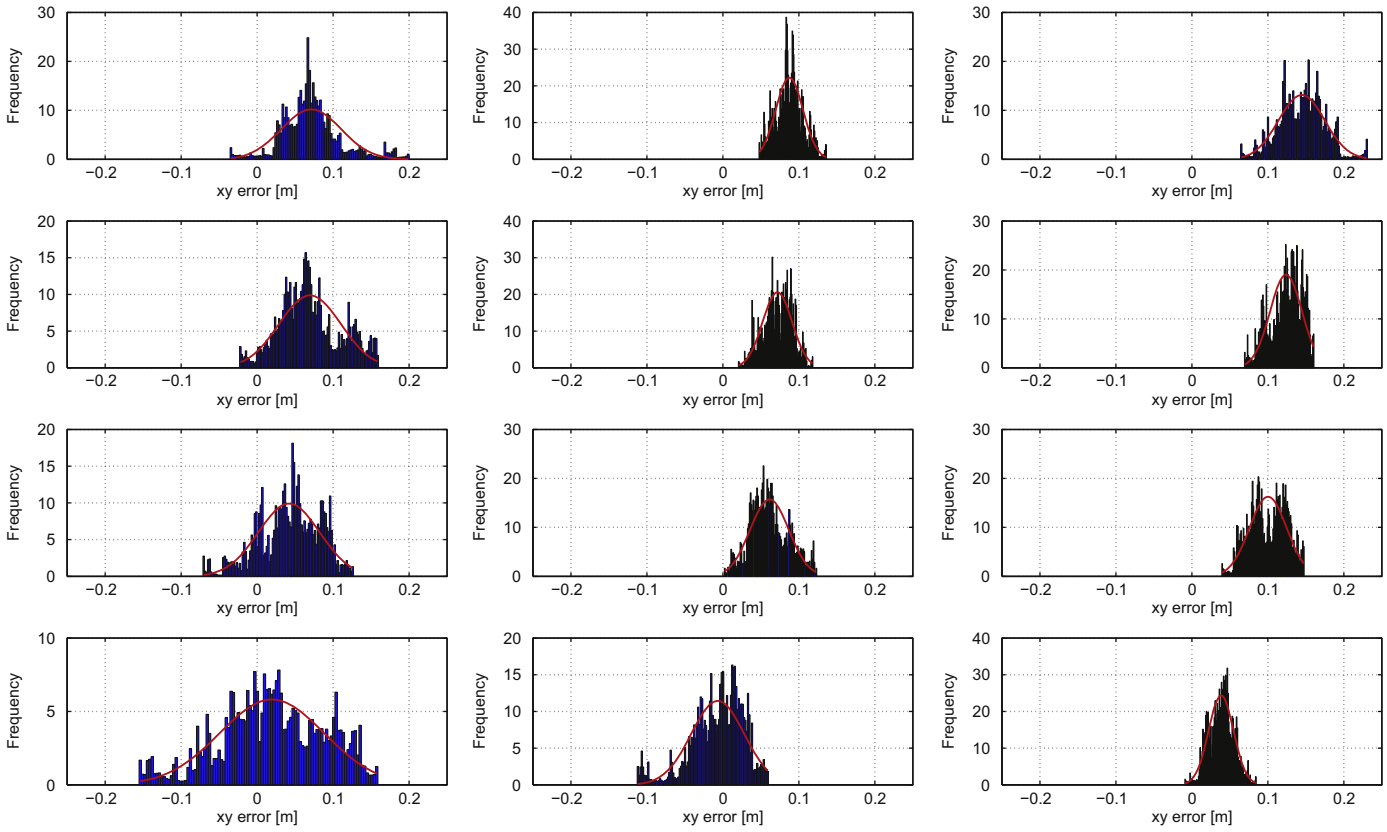

Fig. 21. Histogram of the tracking error along with the fitted normal density function for the trajectories from Fig. 20.

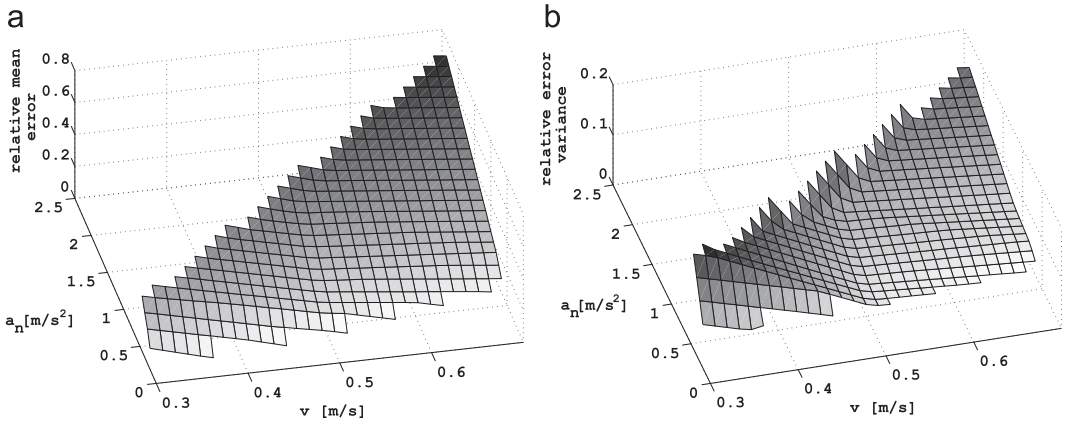

Fig. 22. Mean and variance of the tracking error in the circle tracking experiment: (a) error mean, (b) error variance.

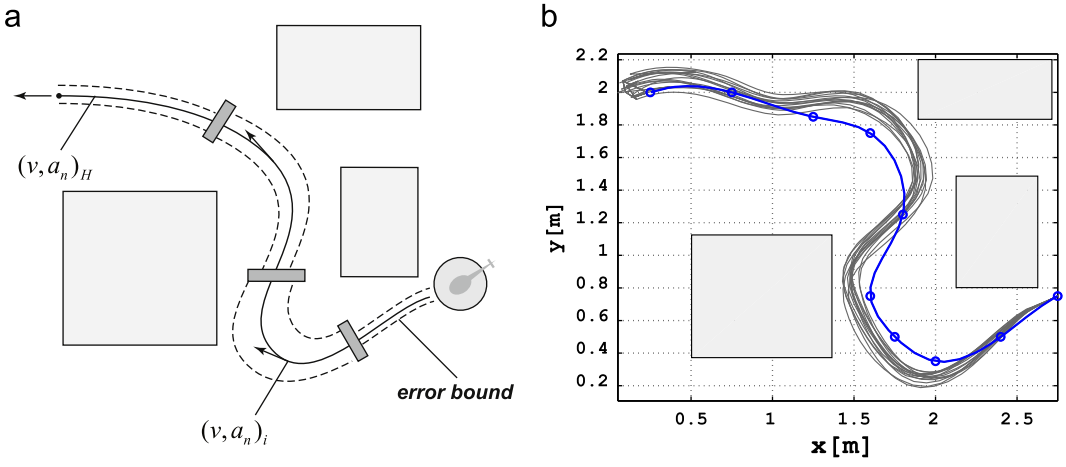

Fig. 23. (a) Illustration of a path in an obstacle-field environment in the presence of tracking errors. (b) 20 Monte-Carlos simulations of the tracking error model showing the waypoints specifying the reference path and the spline fit. Each waypoint has also an attributed reference velocity.

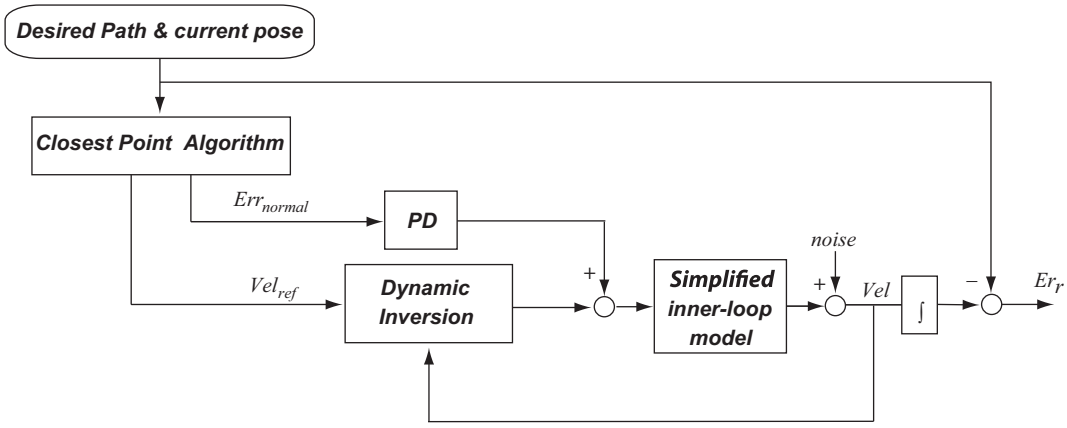

Fig. 24. Block diagram of the tracking error prediction model.

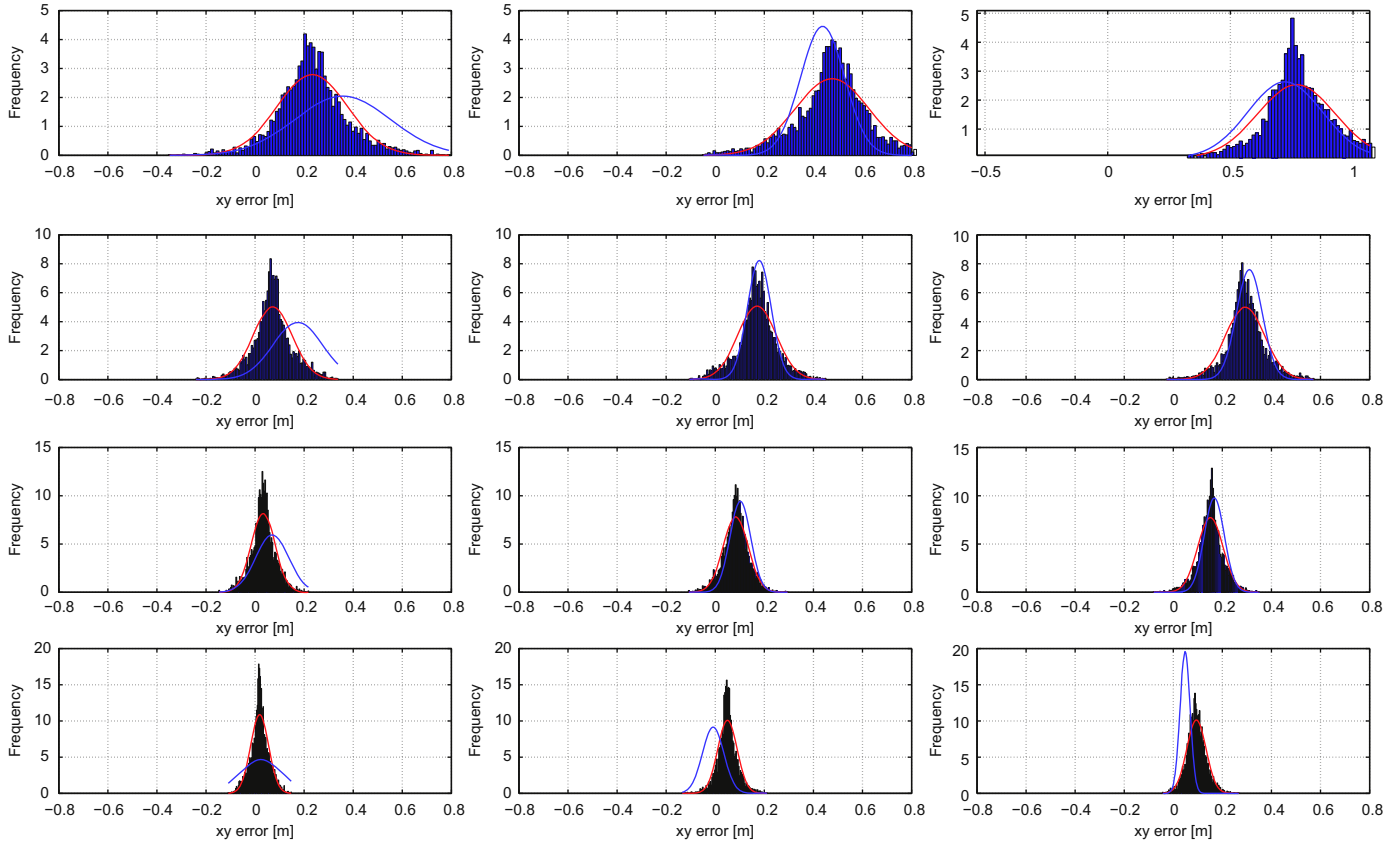

Fig. 25. Histogram of the predicted tracking error along with the experimental statistics (blue). (For interpretation of the references to color in this figure caption, the reader is referred to the web version of this article.)

a comparison between the histogram of the predicted error with the experimental results obtained from the circle experiments.

The differential equation governing the path tracking dynamics can be further simplified. Ignoring the inner-loop transient response, the attitude angles of the helicopter become

$$\theta = \theta_{ref} = X_\theta^{-1}[\dot{u}_{des} - X_u u] + K_p e_x + K_d \dot{e}_x + \eta_x$$
$$\phi = \phi_{ref} = Y_\phi^{-1}[\dot{v}_{des} - Y_v v] + K_p e_y + K_d \dot{e}_x + \eta_y \quad (35)$$

substituting the above equations into the velocity dynamics and assuming perfect dynamic-inversion, the following closed-loop translational dynamics are obtained:

$$\dot{u} = \dot{u}_{des} + K_p e_x + K_d \dot{e}_x + \eta_x$$
$$\dot{v} = \dot{v}_{des} + K_p e_y + K_d \dot{e}_y + \eta_y$$
$$\dot{x} = u$$
$$\dot{y} = v \quad (36)$$

As expected from the analysis in Appendix B, the driving factors in the path following dynamics are the desired tangential acceleration (first term in the right-hand side) and the normal tracking error (second and third terms).

This model is simple enough to be used online. The tracking error bounds can be computed from the equation set (36) running Monte-Carlo simulations based on sample values of the random variables η_x and η_y. The vector $[\dot{u}_{des}, \dot{v}_{des}]$ is computed by differentiating the reference velocity vector (tangent to the path).

Table 1
Parameters of Blade-CX2 coaxial helicopter obtained from system identification techniques along with their Cramer–Rao (CR) bounds.

Param.	Nom. values	CR bound (%)
X_u	−0.446	10.3
A_u	2.289	10.9
X_θ	−9.810	–
$1/\tau$	−36.170	21.0
M_a	189.600	18.7
L_b	265.400	8.7
A_{lon}	−4.157	10.3
B_{lon}	−2.232	8.2
Y_v	−0.604	7.1
B_v	−2.141	8.1
Y_ϕ	9.810	–
$1/\tau'$	−1.789	8.4
M_c	154.500	3.4
L_d	186.200	3.5
A_{lat}	−2.908	10.5
B_{lat}	4.900	7.9

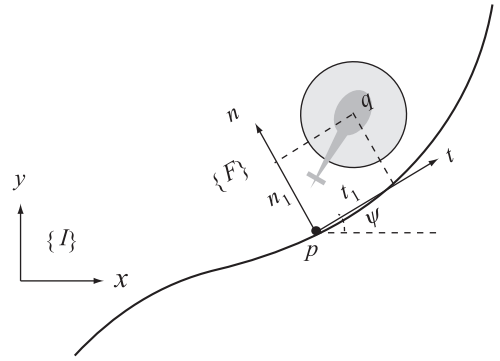

Fig. 26. Illustration of the helicopter in path following problem using a Serret-Frenet coordinate frame (t,n).

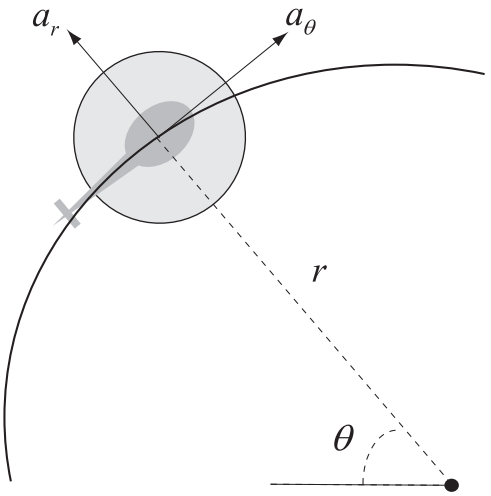

Fig. 27. Description of the helicopter motion on a circular path using radial and transverse coordinates (r,θ).

6. Conclusion

This paper described a systematic approach for designing the entire set of control laws called for by autonomous rotorcraft guidance. These control laws include the attitude dynamics compensation, velocity control augmentation and the path tracking system. The complete system was implemented and evaluated on a miniature coaxial rotorcraft in the Interactive Guidance and Control Lab (IGCL). The overall system performance was then characterized and the results were used to determine a tracking error model that describes the tracking performance over the flight envelope.

The path following system is based on the analysis of the nonlinear rigid-body dynamics. It provides the autonomous rotorcraft the capability to follow a reference trajectory specified by a sequence of waypoints and speeds. Such path references are common in autonomous guidance systems. The path following loop is wrapped around a velocity control system. The complete system augments the vehicle in a way that provides favorable path tracking characteristics. The velocity control augmentation is based on a nested attitude-velocity loop control architecture. It was designed following classical loop-shaping and dynamic inversion techniques using a linear model.

In a first evaluation step, the robust performance and robust stability of the closed-loop system was analyzed using experimental frequency response data combined with parametric modeling uncertainties. These were extracted during the rotorcraft's frequency-domain system identification. In a second evaluation step, flight tests were performed to determine the tracking performance over the flight envelope. The trajectory data was used to extract the tracking error statistics which were used to determine a tracking error model. The model provides a comprehensive perspective on robustness and performance not possible with traditional robust control analysis. Therefore it can be used as a tool to refine the control design. The prediction of the tracking error-bound for a pre-specified path can also be used within a guidance algorithm to tradeoff between maneuver aggressiveness and tracking accuracy, which is essential for safe operation in confined environments.

Acknowledgments

The authors would like to thank Jon Andersh for the support in software and hardware implementation for the base-station.

Appendix A. Blade-CX2 helicopter model

The state-space model for the Blade-CX2 coaxial helicopter is given by

$$
\begin{aligned}
\dot{u} &= X_u u + X_\theta \theta \\
\dot{v} &= Y_v v + Y_\theta \theta \\
\dot{\theta} &= q \\
\dot{\phi} &= p \\
\dot{q} &= M_a a + M_c c \\
\dot{p} &= L_b b + L_d d \\
\dot{a} &= -\frac{a}{\tau} - q + A_{lon} u_{lon} + A_{lat} u_{lon} + A_u u \\
\dot{b} &= -\frac{b}{\tau} - p + B_{lon} u_{lon} + B_{lat} u_{lat} + B_v v \\
\dot{c} &= -\frac{1}{\tau'} c - C_q q \\
\dot{d} &= -\frac{1}{\tau'} d - D_p p
\end{aligned}
\tag{37}
$$

where a and b are the longitudinal and lateral flapping of the lower rotor, respectively. Similarly, c and d are the longitudinal and lateral flapping of the merged upper rotor and stabilizer-bar. In addition, θ and q are pitch angle and pitch rate, ϕ and p are roll angle and roll rate. u and v are longitudinal and lateral velocity components in body frame. The variables u_{lon} and u_{lat} are control inputs. The identified parameters and corresponding Cramer–Rao

(CR) bounds of Blade-CX2 helicopter are shown in Table 1. Details of the Blade CX system identification modeling are available in Dadkhah and Mettler (accepted for publication).

Appendix B. Nonlinear analysis of path following based on point mass model

This section of the appendix addresses the problem of steering a point-mass model along a desired trajectory. The point mass model has the following dynamics:

$$\begin{aligned}\dot{u} &= a_x\\ \dot{v} &= a_y\\ \dot{x} &= u\\ \dot{y} &= v\end{aligned} \tag{38}$$

The input to the system is the accelerations a_x and a_y. Consider the Serret-Frenet frame $\{F\}$ in Fig. 26 as described in Soetanto, Lapierre, and Pascoal (2003) that moves along the path with one axis tangent to the path and another axis perpendicular to the path. The inertial frame is denoted by $\{I\}$. Let also p and q be the origin of the $\{F\}$ frame and vehicle, respectively. In addition, ψ is the path angle, s is the path arc length, κ is the path curvature and $\omega_c = \kappa\dot{s}$ is the angular velocity of the $\{F\}$ frame.

The rotation matrix from the $\{I\}$ frame to the $\{F\}$ frame is given by

$$C_I^F(\psi) = \begin{bmatrix} \cos\psi & \sin\psi \\ -\sin\psi & \cos\psi \end{bmatrix} \tag{39}$$

The inertial velocity of point q in $\{F\}$ can be expressed as

$${}^{F}\left(\frac{dr}{dt}\right) = C_I^F(\psi)\,{}^{I}\left(\frac{dq}{dt}\right) - {}^{F}\left(\frac{dp}{dt}\right)^{F} - {}^{F}(\omega_c \times r) \tag{40}$$

where

$$\begin{aligned}{}^{F}r^{F} &= [t_1, n_1]^T\\ {}^{F}\left(\frac{dp}{dt}\right) &= [\dot{s}, 0]^T\\ {}^{I}\left(\frac{dq}{dt}\right) &= [\dot{x}, \dot{y}]^T\end{aligned} \tag{41}$$

Combining and rearranging Eqs. (39)–(41) yields

$$\begin{aligned}\dot{t}_1 &= \cos\psi\dot{x} + \sin\psi\dot{y} - \dot{s} + \kappa\dot{s}n_1\\ \dot{n}_1 &= -\sin\psi\dot{x} + \cos\psi\dot{y} - \kappa\dot{s}t_1\end{aligned} \tag{42}$$

Combining Eq. (38) with (42), the complete dynamical model for path following is

$$\begin{aligned}\dot{t}_1 &= \cos\psi u + \sin\psi v - \dot{s} + \kappa\dot{s}n_1\\ \dot{n}_1 &= -\sin\psi u + \cos\psi v - \kappa\dot{s}t_1\\ \dot{u} &= a_x\\ \dot{v} &= a_y\end{aligned} \tag{43}$$

Eqs. (43) can be written in the form of

$$\dot{z} = f(z) + g(z)\zeta \tag{44}$$

$$\dot{\zeta} = a \tag{45}$$

where $z = [t_1, n_1]^T$, $\zeta = [u, v]^T$ and $a = [a_x a_y]^T$. Backstepping technique (Khalil, 2003) can be used to find the control law that allows to regulate the tracking error t_1 and n_1. To this end, we first seek a control law of the form $\zeta = \Phi(z)$ to stabilize the system (44). Given a Control Lyapunov Function (CLF) of the form

$$V = \tfrac{1}{2}(t_1^2 + n_1^2) \tag{46}$$

after some manipulations, it can be shown that the following control law:

$$\zeta = \Phi(z) = \begin{bmatrix} u \\ v \end{bmatrix} = \begin{bmatrix} \dot{s}\cos\psi + n_1\sin\psi - t_1\cos\psi \\ \dot{s}\sin\psi - n_1\cos\psi - t_1\sin\psi \end{bmatrix}$$

implies that

$$\dot{V} = -n_1^2 - t_1^2 \le 0 \tag{47}$$

Now in order to take into account the integral action in Eq. (45), let us now state the backstepping lemma (Khalil, 2003):

Lemma 1 (*Backstepping*). *Consider the system (44) and (45) and let $\Phi(z)$ be a stabilizing state feedback law for the system in Eq. (44). Let $V(z)$ be a CLF such that*

$$\frac{\partial V}{\partial z}[f(z) + g(z)\Phi(z)] \le -W(z) \tag{48}$$

for some positive definite $W(z)$. Then the state feedback law of the form

$$a = \frac{\partial \Phi}{\partial z}[f(z) + g(z)\Phi(z)] - \frac{\partial V}{\partial z}g(z) - k[\zeta - \Phi(z)] \tag{49}$$

stabilizes the origin of (44)–(45) with $V(z) + 0.5(\zeta - \Phi(z))^T(\zeta - \Phi(z))$ as a Lyapunov function.

Applying Lemma 1 to the path following problem, it can be show that the following state feedback control law regulates the path tracking error

$$\begin{bmatrix} a_x \\ a_y \end{bmatrix} = -C_F^I(\psi)\begin{bmatrix} t_1 \\ n_1 \end{bmatrix} - \begin{bmatrix} u \\ v \end{bmatrix} \tag{50}$$

The first term in the control law (50) transforms the tangential and normal tracking error to the vehicle reference frame (here it is inertial frame) and the second term adds the velocity feedback. In essence, the control law (50) is a decoupled PD compensator that acts on track and cross-track errors.

Appendix C. Linear analysis of path following around a nominal circular path

This section of the appendix provides the analysis of the path following controller for the point-mass model. The purpose of this analysis is to understand how a linear controller behaves compared to its nonlinear counterpart for the path following problem of the same simplified vehicle model. It is convenient to represent the motion on a circular path using radial-tangential coordinate system as shown in Fig. 27. The equations of motion in this frame are given by

$$\begin{aligned}\ddot{r} - r\dot{\theta}^2 &= a_r\\ r\ddot{\theta} + 2\dot{r}\dot{\theta} &= a_\theta\end{aligned} \tag{51}$$

Linearizing around a nominal circular path $r = r_o$ and $\dot{\theta} = \omega = \omega_o$, we obtain the following linear perturbation state-space model:

$$\frac{d}{dt}\begin{bmatrix} \delta\dot{r} \\ \delta r \\ \delta\omega \\ \delta\theta \end{bmatrix} = \begin{bmatrix} 0 & \omega_o^2 & 2\omega_o r_o & 0 \\ 1 & 0 & 0 & 0 \\ \frac{-\omega_o}{2r_o} & 0 & 0 & 0 \\ 0 & 0 & 1 & 0 \end{bmatrix}\begin{bmatrix} \delta\dot{r} \\ \delta r \\ \delta\omega \\ \delta\theta \end{bmatrix} + \begin{bmatrix} 1 & 0 \\ 0 & 0 \\ 0 & \frac{1}{r_o} \\ 0 & 0 \end{bmatrix}\begin{bmatrix} \delta a_r \\ \delta a_\theta \end{bmatrix} \tag{52}$$

where $\delta\dot{r}$, δr, $\delta\omega$ and $\delta\theta$ are perturbations in radial speed, position, angular rate and angle with respect to the nominal path.

The analysis based on Wang and Davison (1973) shows that the linear state-space model in Eq. (52) can be stabilized by

a decentralized, decoupled state feedback controller of the form

$$\begin{bmatrix} a_r \\ a_\theta \end{bmatrix} = \begin{bmatrix} \times & \times & 0 & 0 \\ 0 & 0 & \times & \times \end{bmatrix} \begin{bmatrix} \delta\dot{r} \\ \delta r \\ \delta\omega \\ \delta\theta \end{bmatrix} \tag{53}$$

Notice that this linear controller describes a decoupled PD controller in radial and tangential axis. The results of this linear analysis are in accordance with the nonlinear analysis in Appendix B.

References

Aguiar, A. P., Dačić, D. B., Hespanha, J. P., & Kokotović, P. (2004). Path-following or reference-tracking? An answer based on limits of performance. In *Proceedings of the 5th IFAC symposium on intelligent autonomous vehicles*, July.

Aguiar, A. P., & Hespanha, J. P. (2007). Trajectory-tracking and path-following of underactuated autonomous vehicles with parametric modeling uncertainty. *IEEE Transactions on Automatic Control*, *52*(August (8)), 1362–1379.

Aguiar, A. P., Hespanha, J. P., & Kokotović, P. V. (2005). Path-following for non-minimum phase systems removes performance limitations. *IEEE Transactions on Automatic Control*, *50*(February (2)), 234–239.

Anon. (1996). *Application of multivariable control theory to aircraft flight control laws*, *final report*: *Multivariable control design guidelines*. Technical Report WL-TR-96 3099, Honeywell and Lockheed Martin Final Report to U.S. Air Force, May.

Balas, G. J., Chiang, R., Packard, A., & Safonov, M. (2005). *Robust control toolbox*. For use with Matlab. Users Guide, Version 3.

Civita, M. L., Papageorgiou, G., Messner, W. C., & Kanade, T. (2006). Design and flight testing of an H_∞ controller for a robotic helicopter. *Journal of Guidance, Control, and Dynamics*, *29*(March (2)).

Conte, G., Duranti, S., & Merz, T. (2004). Dynamic 3D path following for an autonomous helicopter. In *Proceedings of the IFAC symposium on intelligent autonomous vehicles*.

Cunha, R., Antunes, D., Gomes, P., & Silvestre, C. (2006). A path-following preview controller for autonomous air vehicles. In *AIAA guidance*, *navigation*, *and control conference*, Keystone, Colorado, August.

Dadkhah, N., & Mettler, B. (2011). Sensory predictive guidance in partially known environment. In *AIAA guidance*, *navigation*, *and control conference*, Portland, Oregon, August.

Dadkhah, N., & Mettler, B. System identification modelling and flight characteristics analysis of miniature co-axial helicopter. *Journal of American Helicopter Society*, accepted for publication.

Encarnaçao, P., & Pascoal, A. (2001). Combined trajectory tracking and path following: An application to the coordinated control of autonomous marine craft. In *IEEE conference on decision and control* (Vol. 1. pp. 964–969).

Enns, D., & Keviczky, T. (2006). Dynamic inversion based flight control for autonomous RMAX helicopter. In *American control conference*, Minneapolis, MN, June.

Frazzoli, E., Dahleh, M., & Feron, E. (2000). Trajectory tracking control design for autonomous helicopters using a backstepping algorithm. In *American control conference* (Vol. 6, pp. 4102–4107).

Gavrilets, V., Martinos, I., Mettler, B., & Feron, E. (2002). Control logic for automated aerobatic flight of miniature helicopter. In *Proceedings of the AIAA guidance, navigation and control conference*, Monterey, CA, August.

Halaas, D. J., Bieniawski, S. R., Pigg, P., & Vian, J. (2009). Control and management of an indoor, health enabled, heterogeneous fleet. In *AIAA infotech aerospace conference and AIAA unmanned unlimited conference*, Washington, Seattle.

Hoffmann, G., Waslander, S., & Tomlin, C. (2008). Quadrotor helicopter trajectory tracking control. In *AIAA guidance, navigation, and control conference*, Honolulu, HI, August.

Johnson, E., & Kannan, S. (2002). Adaptive flight control for an autonomous unmanned helicopter. In *AIAA guidance, navigation and control conference*, Monterey, CA, August.

Kaminer, I., Pascoal, A., Hallberg, E., & Silvestre, C. (1998). Trajectory tracking for autonomous vehicles: *An integrated approach to guidance and control*. *Journal of Guidance, Control, and Dynamics*, *21*(1), 29–38.

Khalil, H. K. (2003). *Nonlinear systems*. Prentice Hall.

Kim, H., & Shim, D. (2003). A flight control system for aerial robots: *Algorithms and experiments*. *Control Engineering Practice*, *11*(12), 1389–1400.

Kim, H., Shim, D., & Sastry, S. (2002). Nonlinear model predictive tracking control for rotorcraft-based unmanned aerial vehicles. In *American control conference* (Vol. 5, pp. 3576–3581).

Mettler, B. (2002). *Identification modeling and characteristics of miniature rotorcraft*. Boston: Kluwer Academic Publishers.

Mettler, B., Dadkhah, N., & Kong, Z. (2010). Agile autonomous guidance using spatial value functions [Special Issue on Aerial Robotics]. *Control Engineering Practice*, *18*(7), 773–788.

Mettler, B., Dadkhah, N., Kong, Z., & Andersh, J. (2013). Research infrastructure for interactive human-and autonomous guidance. *Journal of Intelligent and Robotic Systems*, *70*(1–4), 437–459.

Mettler, B., Dever, C., & Feron, E. (2004). Scaling and dynamic characteristics of miniature rotorcraft. *AIAA Journal of Guidance Navigation and Control*, *27* (January (3)).

Mettler, B., Tischler, M., Kanade, T., & Messner, W. (2000). Attitude control optimization for a small-scale unmanned helicopter. In *AIAA guidance, navigation and control conference and exhibit*, Denver, CO, August.

Michini, B., & How, J. P. (2009). Adaptive control for indoor autonomous vehicles: Design process and flight testing. In *AIAA guidance, navigation and control conference and exhibit*, Chicago, IL.

Milam, M. (2003). *Real-time optimal trajectory generation for constrained dynamical systems*. Ph.D. Thesis, California Institute of Technology.

Murray, R., Hauser, J., Jadbabaie, A., Milam, M. B., Petit, N., Dunbar, W., et al. (2003). Online control customization via optimization-based control. *Software-Enabled Control*, 149–174.

Pavlov, A., van de Wouw, N., Pogromsky, A., Heertjes, M., & Nijmeijer, H. (2007). Frequency domain performance analysis of nonlinearly controlled motion systems. In *IEEE conference on decision and control*, New Orleans, LA.

Pavlov, A., Wouw, N., & Nijmeijer, H. (2007). Frequency response functions for nonlinear convergent systems. *IEEE Transactions on Automatic Control*, *52*(June (6)).

Petit, N., Milam, M. B., & Murray, R. M. (2001). Inversion based constrained trajectory optimization. In *5th IFAC symposium on nonlinear control systems*.

Press, W. H., Teukolsky, S. A., Vetterling, W. T., & Flannery, B. P. (2002). *Numerical recipes in C++: The art of scientific computing*. Cambridge University Press.

Quigley, M., Gerkey, B., Conley, K., Faust, J., Foote, T., Leibs, J., et al. (2009). ROS: An open-source robot operating system. In *Proceedings of open-source software workshop on international conference on robotics and automation* (*ICRA*), Kobe, Japan.

Raptis, I., Valavanis, K., & Moreno, W. (2011). A novel nonlinear backstepping controller design for helicopters using the rotation matrix. *IEEE Transactions on Control Systems Technology*, *19*(March (2)), 465–473.

Raptis, I. A., & Valavanis, K. P. (2011). Linear and nonlinear control of small-scale unmanned helicopters. In *International series on intelligent systems*, *control and automation*: *Science and engineering* (Vol. 45). Springer.

Schafroth, D., Bermes, C., Bouabdallah, S., & Siegwart, R. (2010). Modeling, system identification and robust control of a coaxial micro helicopter. *Control Engineering Practice*, *18*, 700–711.

Skogestad, S., & Postlethwaite, I. (2005). *Multivariable feedback control analysis and design*. John Wiley and Sons.

Soetanto, D., Lapierre, L., & Pascoal, A. (2003). Adaptive, non-singular path-following control of dynamic wheeled robots. In *IEEE conference on decision and control* (pp. 1765–1770).

Spenko, M., Kuroda, Y., Dubowsky, S., & Iagnemma, K. (2006). Hazard avoidance for high-speed mobile robots in rough terrain. *Journal of Field Robotics*, *23*(5), 311–331.

Takahashi, M. D., Schulein, G., & Walley, M. (2008). Flight control law design and development for an autonomous rotorcraft. In *Proceedings of the 64th forum of American Helicopter Society*, May.

Tischler, M., & Cauffman, M. (1994). *Comprehensive identification from frequency responses* (*CIFER*): *An interactive facility for system identification and verification*. Technical report, NASA CP 10149, USAATCOM TR-94-A-017, September.

Tischler, M., Colbourne, J., Morel, M., Biezad, D., Cheung, K., Levine, W., et al. (1999). A multidisciplinary flight control development environment and its application to a helicopter. *IEEE Control Systems Magazine*, *19*(August (4)), 22–33.

Tischler, M. B., & Remple, R. K. (2006). Aircraft and rotorcraft system identification, engineering methods with flight test examples. In *AIAA education series*.

U.S. Army Aviation and Missile Command (2000). *Handling qualities requirements for military rotorcraft*, ADS-33E-PRF. Aviation Engineering Directorate, March.

van Nieuwstadt, M. J. (1996). *Trajectory generation for nonlinear control systems*. Ph. D. Thesis, California Institute of Technology.

Wang, S. H., & Davison, E. J. (1973). On the stabilization of decentralized control systems. *IEEE Transactions on Automatic Control*, *18*(5), 473–478.